LES of explosions in venting chamber: a test case for premixed turbulent combustion models

Olivier Vermorel[a,*], Pierre Quillatre[a,b,1], Thierry Poinsot[c]

[a] *CERFACS, CFD Team, 42 Avenue G. Coriolis, 31057 Toulouse Cedex 01, France*
[b] *TOTAL S.A., Tour Coupole, 92078 Paris La Défense Cedex, France*
[c] *Institut de Mécanique des Fluides de Toulouse, CNRS, Avenue C. Soula, 31400 Toulouse, France*

Abstract

This paper presents a new experimental and Large Eddy Simulation (LES) database to study upscaling effects in vented gas explosions. The propagation of premixed flames in three setups of increasing size is investigated experimentally and numerically. The baseline model is the well-known laboratory-scale combustion chamber from Sydney (Kent *et al.* 2005, Masri *et al.* 2012); two exact replicas at scales 6 and 24.4 were set up by GexCon (Bergen, Norway). The volume ratio of the three setups varies from 1 to more than 10 000, a variation unseen in previous experiments, allowing the exploration of a large range of Reynolds and Damköhler numbers. LES of gaseous fully premixed flames have been performed on the three configurations, under different operating conditions, varying the number of obstacles in the chamber, their position and the type of fuel (hydrogen, propane and methane). Particular attention is paid to the influence of the turbulent combustion model on the results (overpressure, flame front speed) comparing two different algebraic sub-grid scale models, the closures of Colin *et al.* (2000) and Charlette *et al.* (2002), used in conjunction with a thickened flame approach. Mesh dependency is checked by performing a highly resolved LES on the small-scale case.

*Corresponding author
Email address: vermorel@cerfacs.fr (Olivier Vermorel)
[1] Present adress: ENGIE Lab - CRIGEN, 361 Avenue du Président Wilson, 93210 Saint-Denis La Plaine, France

For a given scale and with a fixed model constant, LES results agree with experimental results, for all geometric arrangement of the obstacles and all fuels. However, when switching from small-scale cases to medium-scale or large-scale cases this conclusion does not hold, illustrating one of the main deficiencies of these algebraic models, namely the need for an *a priori* fitting of the model parameters.

Although this database was initially designed for safety studies, it is also a difficult test for turbulent combustion models.

Keywords: gas explosion, Large Eddy Simulation, turbulent combustion model, efficiency function

---

1. Introduction

During the explosion of a premixed gas cloud, the first issue is the pressure increase (the so-called overpressure) which controls the severity of the explosion and its impact on surrounding structures. This overpressure can be devastating, causing fatalities and the destruction of large parts of industrial facilities. These phenomena are difficult to predict since they result from a complex and fully unsteady interaction between flame propagation, turbulence and geometry. They occur over a large spectrum of spatio-temporal scales and turbulent combustion regimes. Research in this domain started in the 1970s with the primary objective to develop know-how and tools for predicting and minimizing the effect of accidental explosions [1]. This goal was first reached thanks to experimental campaigns and only recently using computational sciences and resources. Safety Computational Fluid Dynamics (SCFD) is thus a relatively new field of research. As for many applications dealing with turbulence and combustion, e.g. gas turbine or piston engine applications, the standard numerical approach was and still is the (Unsteady) Reynolds Averaged Navier-Stokes (U)RANS approach, at least within industry. This technique gradually replaces simple scaling laws, which were formerly used for interpolation and scaling of experimental data and were shown to be largely inapplicable especially for explosion venting, mainly

because of the small scale of the experimental data on which they are based and because of their inadequate treatment of turbulence generated by leaks and obstacles [1, 2]. Even if URANS codes are able to give correct predictions of the observed experimental trends, they generally contain empirical coefficients which have to be tuned in order to give reasonable results [3, 4]. The need for better prediction capabilities combined with the growing computational power have made Large Eddy Simulation (LES) an alternative and attractive solution. Indeed, LES has the intrinsic capability to give more reliable predictions than URANS methods, as shown by many authors in gas turbine [5, 6, 7, 8] or piston engine applications [9, 10, 11].

The typical research configurations used to study gas explosions consist in vessels with obstacles filled with a premixed flammable mixture. The flame is ignited and first propagates in a laminar way in a flow initially at rest. This laminar phase is followed by a turbulent propagation phase due to the interaction of the front with the obstacles and the turbulence generated behind the obstacles by the expanding gases. This flame-induced turbulence increases combustion intensity, leading to flames which can propagate at several hundreds of m/s while they are of the order of 0.5 m/s in a "normal" laminar flame. In the worst scenario, the initial deflagration flame can transition to detonation. This self-acceleration by obstacle-generated turbulence is responsible for many severe industrial explosions, for example on offshore platforms [1, 12, 13, 14].

Even if detonation is not triggered, a LES SCFD code must be able to handle different combustion regimes, from laminar to turbulent, and their transition. This situation is of course not restricted to explosion phenomena and is very common in many combustion systems using ignition devices such as internal combustion engines or aeronautic engines. Accurate predictions of flame propagation can be achieved only with reliable models for turbulent combustion which are the weakest element in simulation sub-models. The turbulent combustion models developed for LES of reacting flows [15, 16, 17, 18, 19, 20] all rely on

modeling assumptions based on upscaling laws developed under Kolmogorov-type assumptions for turbulence scales [21, 22, 23]. Experimental databases are required to assess their strengths and weaknesses but they remain rare and delicate to build, even for the simplest flows. Most available experimental data for turbulent combustion correspond to flows taking place at atmospheric pressure in vessels of the order of a few liters: the volume of most car engines chambers vary from 0.1 to 2 liters and gas turbines chambers are only slightly larger. When larger chambers are used (furnaces for example), measurements become difficult. In terms of models, this means that the range of Damköhler and Reynolds numbers explored with these systems remains narrow [24, 25, 22]. Consequently, all turbulent combustion models are tested over a limited range of scales so that even wrong models can work without revealing their limitations because no experimental data is available to challenge them. Even DNS can not help because the range of spatio-temporal scales which are reached in DNS remains narrow and does not allow upscaling tests [26, 22]. Furthermore, many experimental configurations used for model validation, such as turbulent bombs or steady burners, suffer from the same limitations: results depend strongly on the turbulence, either present at ignition time (for turbulent bombs) or injected at the inlet (for steady burners). Finally, LES in large domains are quite difficult to perform without massive computing capacities.

In order to help developing and validating turbulent combustion models, a new experimental database (called SydGex in the following) is presented in this paper. Although originally designed for safety studies, its usefulness may go well beyond this initial application. The database consists in a set of three experiments of exactly similar shapes and increasing size scaled by 1, 6 and 24.4. The smallest experiment is the vented explosion chamber from Sydney University [27, 28]. This is a square cross section chamber filled with various obstacles (1 to 3 baffle plates plus a central square cross section obstacle). Compared to other laboratory-scale experiments [29, 30, 31, 32, 33, 34, 35, 36, 37], this configuration is characterized by a small volume of 0.625 liter (while the volume

in the above references typically ranges from 2.98 liters [29] to 56.3 liters [31]), a relatively low length to diameter (or height) ratio of 5 (ratios from 2 [31] to 32 [36] in the above references) and an intermediate blockage ratio of 0.24 for the baffle plates and 0.5 for the central obstacle (ratios from 0.2 [32] to 0.8 [32] in the above references). This is also one of the few experiments (with [32]) which provides data for various fuels, namely propane, methane and hydrogen. This configuration is particularly well suited for LES and model validation:

- As mentioned before, the dimensions of the combustion chamber are small and perfectly compatible with LES and the current computational resources.

- Initial conditions are perfectly defined: the flow is at rest. For decades, the question of initial conditions has been a major limitation of our capacity to evaluate models for turbulent premixed flames. If the turbulence in which the flame develops is not known with precision, it is impossible to validate a model because a simple tuning of the initial turbulent flow is sufficient to match the experimental flame speed. For example, most turbulent flames propagating in fan-stirred bombs have suffered from this limited precision in terms of initial turbulent state [38, 39, 40].

- Boundary conditions are also well defined. The thermal conditions on the walls are clear since walls do not have enough time to heat up and their temperature remains equal to the initial temperature.

This configuration has already been extensively studied with LES. Gubba and co-workers obtained very convincing results for a propane-air mixture [41, 42, 43, 44]. A wide range of configurations were computed to explore various aspects such as the effects of location and number of the solid obstacles as well as area blockage ratio. In these studies an algebraic flame surface density model was considered in order to account for the unresolved part of the sub-grid scale reaction rate, either with a constant-based formulation or a dynamic one. It was found that the LES predictions are slightly improved by the use of the dy-

namic procedure [42, 44]. In [45], this work was extended to a lean hydrogen-air mixture. Accurate predictions of the flame shape and peak overpressure were again obtained for different numbers and locations of obstacles.

The two other experiments (performed by GexCon in Norway) are scaled-up versions of the Sydney test rig at scale 6 and 24.4. With a volume of 135 and 9 079 liters respectively, these two new configurations largely exceed the size of classical laboratory-scale experiments discussed above. The corresponding volume ratio of the combustion chamber then varies from 1 (for the Sydney case) to 216 for the medium-scale case and to 14 526 for the large-scale case, a range which has never been reached before in any turbulent combustion experiment. Since the geometry and the operating conditions of the three setups are the same, the only parameters changing from one case to another are the values of the Damköhler and Reynolds numbers. This database thus constitutes a unique set of results to address the overarching problem of turbulent combustion: how to write a good turbulent combustion model and validate it over a wide range of scales? Here, the conditions reached in the SydGex database in a classical turbulent combustion diagram (Fig. 1) cover a much wider range than what is observed in all canonical bombs or engines: u'/S_l^0 can reach 20, l_t/δ_l^0 is of the order of 1500 and, even if detonation is never triggered, flame fronts can propagate at velocities close to 400 m/s (these figures are extracted from the simulations described thereafter).

The method used here to analyze the performance of the LES turbulent combustion models differs from what is done usually for steady burners for example, where one or two regimes are tested extensively using full fields of velocity, species and temperature [15, 46, 7]. For venting chambers, the main qualitative indicator of the model quality is the flame position visualization (which provides a flame speed) and the quantitative data to capture is the pressure curve versus time which is controlled by two phenomena: the overall combustion rate and the mass flow rate at the venting chamber exit. The

pressure curve is very sensitive to the reaction rate which is the quantity we want to investigate. No comparison with velocity, temperature or species field will be performed here but this is compensated by the fact that the comparison is not performed for one or two regimes but for more than 10 cases where the overall size of the setup, the fuel type and the configuration (number and location of obstacles) will be changed systematically.

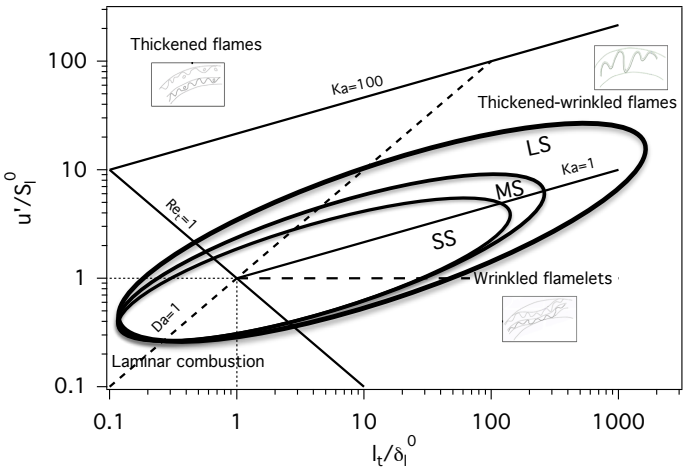

Figure 1: Classical turbulent combustion diagram for premixed turbulent flames [22, 23] as a function of the length ratio (turbulence integral scale l_t/ flame thickness δ_l^0) and velocity ratio (rms (root mean square) velocity u'/ flame speed S_l^0). The approximate locations of the SydGex database are indicated by the three oval curves: Sydney's small-scale experiment (SS), GexCon's medium-scale experiment (MS) and GexCon's large-scale experiment (LS).

The SydGex database is presented in Section 2. The setup of the small-scale Sydney experiment is briefly recalled before presenting the two replicas at medium- (Sydney's experiment $\times 6$) and large-scale (Sydney's experiment $\times 24.4$). The LES code and sub-grid models are described in Section 3. LES of different operating conditions were performed, varying the number of obstacles, their position and the type of fuel (hydrogen, propane and methane). Sections 4 (small-scale simulations) and 5 (medium-scale and large-scale simulations) focus

on the influence of the turbulent combustion model comparing two different sub-grid scale models, namely the algebraic closures of Colin *et al.* [47] and Charlette *et al.* [48], used in conjunction with the Thickened Flame (TF) approach [47]. This exercice is similar to that done by Di Sarli *et al.* [49] or Wen *et al.* [50], except that their comparison of various sub-grid scale combustion models relied on only one configuration, whereas many different configurations of varying geometry and size are used here to provide a more challenging assessment of turbulent combustion models.

2. Experimental setup

The SydGex database contains three experimental setups: the Sydney experiment called 'original' or 'small-scale' (SS) (0.25 m long) configuration and its two upscaled versions, the 'medium-scale' (MS) (1.5 m long) and 'large-scale' (LS) (6.1 m long) configurations of GexCon.

2.1. Small-scale experiment

The original Sydney experiment [27, 28] is sketched in Fig. 2. This semi-

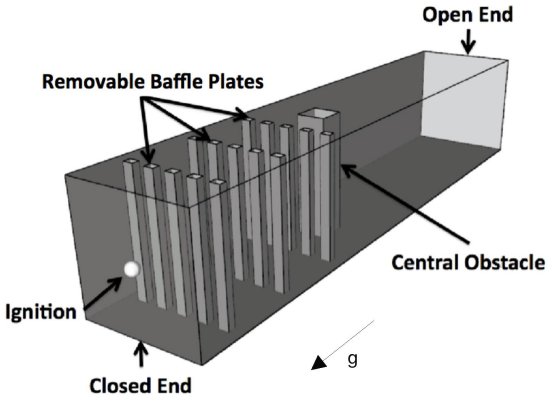

Figure 2: Explosion chamber configuration of Sydney [27, 28]. The vessel is orientated vertically in the experiment: the bottom end of the vessel is on the left of the figure and the top end on the right.

confined configuration consists in a square cross section ($0.05 \times 0.05\ m^2$), 0.25 m long chamber with solid obstacles. Its volume is 0.625 liter. Three removable baffle plates can be placed at various distances from the ignition source (overall blockage ratio of 0.4) while the central square obstacle (1.2 cm square, blockage ratio of 0.24) is fixed [28]. The bottom end of the chamber is closed and the top end is opened out to the atmosphere. The vessel is initially filled with a premixed mixture of fuel and air at atmospheric pressure and temperature. The mixture is then ignited by laser at the closed end. Experimental results include pressure signals and flame front visualizations for three different fuels, namely hydrogen (equivalence ratio Φ=0.7), LPG (95% C_3H_8, 4% C_4H_{10} and 1% C_{5+} hydrocarbons by volume) (Φ=1.0), and CNG (88.8% CH_4, 7.8% C_2H_4,1.9% CO_2 and 1.2% N_2 with the remaining 0.3% being a mixture of propane, propene, butane and pentane) (Φ=1.0) [28].

The arrangement of the baffle plates control the flame speed, the flame front shape and the generated overpressure. The nomenclature of [28] is used here to name the different configurations: for example, a configuration named BBOS refers to baffle plates (B) at the first two locations (i.e., close to the ignition point) and a small central obstacle (S) while configuration OOBS refers to a unique baffle plate located close to the central obstacle. For each configuration, the experiment was repeated at least 30 times to obtain reliable results. The configurations computed by LES in Section 4 are summarized in Table 1: they allow to study the influence of the number of grids (OOBS versus OBBS and BBBS), the influence of the position of the grids (BOOS versus OOBS) and the influence of the fuel (LPG versus PNG and H_2).

2.2. Medium- and large- scale experiment

The medium- and large-scale experiments have been set up by GexCon in 2012. Almost all the available measurements and diagnostics are shown in this paper, a few additional results being available in [51]. Raw data are available upon request.

	Configuration			
Fuel	*BBBS*	*OBBS*	*OOBS*	*BOOS*
LPG	✓	✓	✓	✓
CNG	✓			
H_2	✓			

Table 1: Configurations studied for the small-scale (SS) experiment of Sydney [28].

The medium-scale experiment is a replica of the small-scale experiment of Sydney at scale 6. The combustion chamber is a 1.5 × 0.3 × 0.3 m volume (135 liters) with a vent opening. Contrary to the Sydney experiment where the vessel was oriented vertically, the vessel was positioned horizontally on a table due to the higher intensity of the explosion. The three aluminium grids were positioned vertically inside the vessel. All dimensions of the MS rig (Fig. 3)

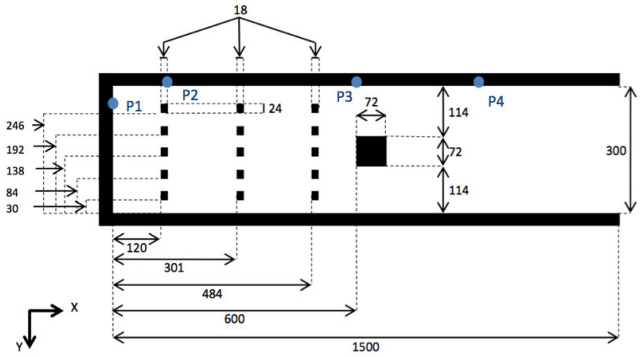

Figure 3: Top view of the medium-scale (MS) test vessel. Measurements are given in mm. The dots indicate the positions of the four pressure transducers (P1 to P4).

correspond to the dimensions of the SS experiment at scale 6 (within a margin of 4% due to the manufacturing process).

The large-scale experiment at GexCon (Fig. 4) is a replica of the Sydney small-scale experiment at scale 24.4, leading to a 6.1 × 1.22 × 1.22 m (9 079 liters) vessel. The vessel is positioned horizontally, directly on the ground. The

removable grids are made out of steel.

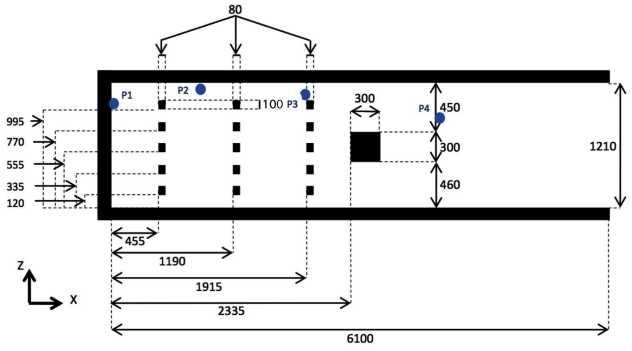

Figure 4: Top view of the large-scale (LS) test vessel. Measurements are given in mm. The dots indicate the positions of the four pressure transducers (P1 to P4).

The explosion experiments were performed with stoichiometric mixtures of methane and propane in air. For the MS tests, class 2.5 methane and propane were used whereas industrial propane was used for the LS tests. In order to contain the gas mixture within the vessel during mixing and filling, the open end was covered with a thin plastic sheet. During the MS tests the plastic foil was clamped over the vent opening and was not removed prior to ignition. For the LS tests, the plastic foil was held in place by a pneumatic system and released just before ignition. Two different ignition sources were used. For the MS tests, a single spark generator based on a car coil was used. In this case, the spark activates immediately after it is triggered. For the LS tests, ignition is performed with an oscillating spark, which ignites the mixture 5 to 25 ms after it is triggered. Additional details are given in Table 2.

The overpressure was measured using 4 piezo-electric pressure transducers from Kistler (type 7261 for the LS experiment and 701A for the MS experiment) connected to Kistler charge amplifiers (type 5073 for the LS experiment and 5011A for the MS experiment). The 7261 and 701A transducers have a frequency response of 13 kHz and 70 kHz respectively. The position of the pres-

	MS	*LS*
Composition	- Class 2.5 propane (99.5% purity), Φ=1 - Class 2.5 methane (99.5% purity), Φ=1	- Industrial propane (95% purity), Φ=1
Ignition system	Spark generator (car coil)	Oscillating spark
Electrodes location	15mm from the wall	50mm from the wall
Interelectrode distance	4mm	4mm

Table 2: Mixture composition and ignition system used in the MS and LS configurations.

sure transducers P1 to P4 is given in Figs. 3 and 4. In practice the four pressure signals are always very similar: since P1 is closest to the position of the pressure transducer used in the SS configuration, only the pressure signal extracted at this position will be shown in the following sections.

The MS tests were recorded using a Phantom v210 high-speed camera at 2000 fps with full resolution of 1280 $\times$ 800 in color. For the MS case, a fast LED light-box unit was lit in parallel with the ignition source to measure flame propagation speeds from the high-speed video recordings. For the LS experiment, video recording was impossible and the pressure-time traces are the only experimental material available for LES validation.

Due to their size, the MS and LS experiments are more delicate to setup and much more costly than the SS experiment. For this reason, the number of configurations studied was reduced compared to the original database of Masri *et al.* The number of shots for each configuration was also reduced: instead of 30 (or more) shots for each configuration of the SS experiment, only 2 to 6 shots were performed here: all shots showed a quite good repeatability with low cyclic variations (see [51] for more details). As an illustration, Fig. 5 shows the overpressure-time traces of three shots performed on the MS test rig for the BBBS configuration (C_3H_8, Φ=1). The peak pressure (810, 824 and 873

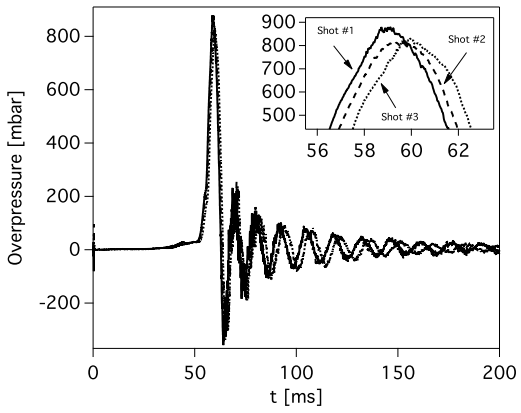

Figure 5: Experimental overpressure-time traces for the three shots performed on the MS test rig for the BBBS configuration (C_3H_8, Φ=1).

mbar), its rate of change (maximum values of 240, 286 and 294 bar.s$^-$1), and the time taken to reach the peak (59.5, 60.1 and 59.3 ms) are very similar from one shot to another. Similar results were obtained for all configurations for the peak pressure and its rate of change but larger variations were observed for the time to reach peak pressure, probably due to variations in the ignition system. To remove any doubt about the results, this quantity was not used for LES validation. All pressure-time traces plotted in the following sections will thus be shifted in time by a quantity $\Delta t_{peak} = t_{peak}^{LES} - t_{peak}^{exp}$ in order to match the experimental peak pressure instant t_{peak}^{exp} (in practice all LES peak pressure instants t_{peak}^{LES} are larger than the experimental peak pressure instants t_{peak}^{exp}). Note that the uncertainties mentioned here are much smaller than the variations which are investigated: for example, the mean peak pressure for the SS BBBS configuration is about 110 mbar, it reaches 800 mbar for the MS BBBS and 1600 mbar for the LS BBBS configurations.

The test matrices available for LES validation on the MS and LS experiments are shown in Tables 3 and 4.

	Configuration			
Fuel	*BBBS*	*OBBS*	*OOBS*	*BOOS*
LPG	✓	✓	✓	
CNG	✓			
H_2				

Table 3: Configurations studied for the medium-scale (MS) experiment of Gexcon.

	Configuration			
Fuel	*BBBS*	*OBBS*	*OOBS*	*BOOS*
LPG	✓		✓	
CNG	✓			
H_2				

Table 4: Configurations studied for the large-scale (LS) experiment of Gexcon.

3. Numerical setup

The solver used for all LES is AVBP [52, 53, 54, 7]. All computations have been performed with the same numerical setup. The computations only differ by the scale (SS, MS or LS) and the fuel (and its corresponding chemical scheme). AVBP solves the unsteady compressible and reactive multi-species Navier-Stokes equations on unstructured grids. It is a cell-vertex/finite element code, explicit in time. Simulations are performed with the TTGC finite element Taylor-Galerkin convective scheme [55], which is 3^{rd} order in space and time and has a low dissipative error. The diffusion operator (2Δ stencil) relies on a vertex centered formulation combined with a finite element discretization. This operator predicts correct dissipation levels at the smallest resolved scales and dampens high wavenumber oscillations [56]. An explicit time-integration is used for the species chemical source terms with a finite-element based spatial discretization [56]. Gravity is not accounted for in the LES since its contribution in the momentum and energy equations is much lower than the contributions

of the different fluxes and source terms.

The different models used in all computations are listed below:

- Sub-grid scale turbulence is modeled by the WALE viscosity based model [57].
- Chemistry is modeled by reduced schemes [58] which match the laminar flame speed, the flame thickness and the burnt gases adiabatic temperature. CNG and LPG have been replaced by their main respective component in the computations: CNG was replaced by CH_4 (88.8% of CNG volume) and LPG by C_3H_8 (95% of LPG volume). Given the experimental uncertainties relative to the mixture (actual composition of LPG and CNG, equivalence ratio, supposedly perfectly premixed mixture) and, more basically, given the classical uncertainties found in the literature regarding laminar flame speeds (even for the simplest fuels such as CH_4 or C_3H_8, discrepancies of 5% to 10% are often observed), this simplification seems reasonable. Three different reduced chemical schemes have thus been used: two two-step reduced schemes for CH_4-air and C_3H_8-air combustion (oxydation and CO-CO_2 equilibrium) and one one-step reduced scheme (oxydation only) for H_2-air combustion [51].
- Ignition is a complex phenomenon (plasma formation, shock waves, radiative effects, ...) and its modeling is a task that extends far beyond the scope of this study. Here, calculations are initialized by a small hemisphere of burnt gases (radius 1 cm) at the ignition point. This model is acceptable here since it mainly impacts the time to reach the peak pressure (a quantity which we are not interested in, see Section 2) and not the magnitude of the peak pressure itself [45]. Furthermore it matches well the real conditions of ignition: since the flow is at rest initially, assuming that the flame will still be laminar and hemispherical when it reaches a 1 cm radius is reasonable.

- The combustion model associates the Thickened Flame for LES (TFLES) approach [47, 59, 60, 19] to resolve the flame front on the computational mesh and an efficiency function to account for the loss of wrinkling at the sub-grid scale due to flame thickening. While various other models have been used for explosions [49, 43, 61, 50, 62], we focus on methods which explicitly resolve the inner flamelet structure in order to capture curvature, strain and non adiabaticity effects. The thickening factor $\mathcal{F}$ is computed in a dynamic way: it is maximum in flame zones and decreases to unity in non reactive zones, using a flame sensor depending on the local temperature and mass fractions [59]. Two different efficiency functions have been tested, namely the formulation of Colin *et al.* [47] and that of Charlette *et al.* [48]. The efficiency function is defined as the wrinkling Ξ_Δ ratio between the non-thickened reference flame and the thickened flame:

$$\mathcal{E} = \frac{\Xi_\Delta(\delta_l^0)}{\Xi_\Delta(\mathcal{F}\delta_l^0)} \tag{1}$$

where δ_l^0 is the laminar flame thickness (calculated from the temperature gradient) of the non-thickened flame and $\mathcal{F}$ is the thickening factor. δ_l^0 is considered as constant during the whole computation, neglecting the effect of the overpressure. It is equal to 0.34 mm for C_3H_8-air cases, 0.41 mm for CH_4-air cases and 0.12 mm for H_2-air cases.

In the formulation of Colin *et al.*, the wrinkling factor Ξ_Δ is defined as:

$$\Xi_\Delta = 1 + \beta_{Colin}\frac{2ln(2)}{3c_{ms}\left[Re_t^{1/2}-1\right]}\Gamma_{Colin}\left(\frac{\Delta}{\delta_l^0},\frac{u'_\Delta}{S_l^0}\right)\frac{u'_\Delta}{S_l^0} \tag{2}$$

where Γ_{Colin} is a function describing the ability of vortices to effectively wrinkle the flame front. S_l^0 is the laminar flame speed (equal to 38.4 cm.s^{-1} for C_3H_8-air cases, 36.3 cm.s^{-1} for CH_4-air cases and 128.0 cm.s^{-1} for H_2-air cases), Δ is the filter size, u'_Δ is the sub-grid scale turbulent velocity, Re_t is a Reynolds number based on u'_Δ and on an estimation of the turbulent integral length scale l_t, and $c_{ms} = 0.28$. For the present computations, l_t is estimated to be equal to the spacing between two bars

of a baffle plate (i.e. 5mm at SS, 30mm at MS and 122mm at LS). β_{Colin} is a model parameter usually set to 0.3 [46, 63, 64, 65, 66].
In the formulation of Charlette *et al.*, the wrinkling factor has an exponent expression:

$$\Xi_\Delta = \left(1 + min\left[\frac{\Delta}{\delta_l^0}, \Gamma_{Charlette}\left(\frac{\Delta}{\delta_l^0}, \frac{u'_\Delta}{S_l^0}, Re_\Delta\right)\right]\right)^{\beta_{Charlette}} \quad (3)$$

where $\Gamma_{Charlette}$ plays a role equivalent to Γ_{Colin} and Re_Δ is the sub-grid scale turbulence Reynolds number. As for the Colin *et al.* expression, a model parameter $\beta_{Charlette}$ has to be specified. Following the original paper of Charlette *et al.* [48], $\beta_{Charlette}$ is set to 0.5.
These algebraic closures for the flame wrinkling potentially have two drawbacks for the simulations of explosions:

- a conceptual drawback, since they assume an equilibrium between turbulence motions and flame wrinkling, an hypothesis which is not justified during the whole explosion scenario, as the flame is laminar at early stages, wrinkling up slowly before reaching a fully turbulent regime.
- a practical drawback, linked to the previous point, since the outcome of these models highly depends on the value of the model parameters β_{Colin} or $\beta_{Charlette}$.

The computational domain includes the venting chamber and a plenum, located at its outlet, which mimics the atmosphere. For all configurations, meshes are made of tetrahedral elements. The number of elements is constant for all LES configurations at all scales, around 20 millions. Figure 6 shows a typical mesh for configuration BBBS SS. In the first two thirds of the combustion chamber (x<160mm), the mesh resolution Δ_x (calculated from the nodal volume) is about 0.5, 3 and 12.2 mm respectively for the SS, MS and LS experiments. This mesh density has been chosen in order to ensure that the flame, even thickened, remains thinner than the distance between the bars of a baffle plate. As an example, for C_3H_8-air LES, the resulting maximum thickening factors $\mathcal{F}$ are

of the order of 7.3 at SS, 44 at MS and 179 at LS (the flame is resolved on 5 grid points). The mesh is progressively coarsened in the last third of the chamber, well after the central obstacle. The resolution at the exit of the combustion chamber reaches 1.5, 9 and 37 mm respectively for the SS, MS and LS configurations.

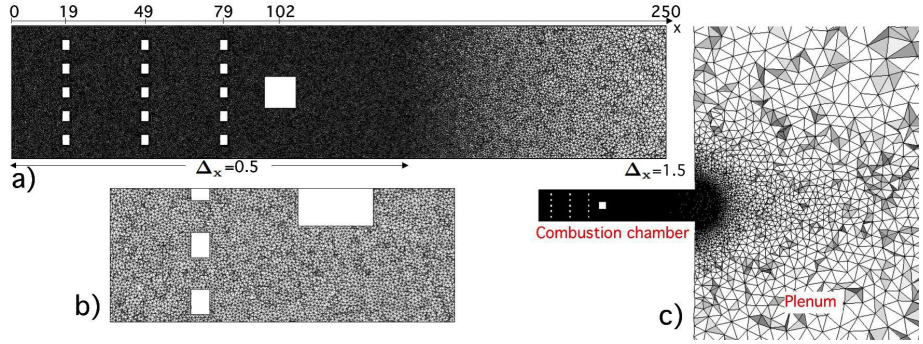

Figure 6: Longitudinal cuts of the mesh passing through the middle of the combustion chamber for configuration BBBS SS. **a)** combustion chamber. **b)** zoom around the third baffle plate and the central obstacle. **c)** global view of the computational domain including the plenum which mimics the atmosphere. All dimensions are in mm.

The whole domain is initialized at rest. The venting chamber is initialized with a perfectly premixed mixture (Φ=1.0 for cases with CH_4-air or C_3H_8-air mixtures, Φ=0.7 for H_2-air mixtures) at atmospheric pressure and temperature. The plenum is filled with air only. The walls of the venting chamber and the obstacles are modeled as non-slip walls. Navier-Stokes Characteristic Boundary Conditions (NSCBC) [67, 68] are used on the borders of the plenum.

All LES were performed on 4 096 processors of the BlueGene/Q machine Turing from GENCI-IDRIS. For SS configurations, about 15ms of physical time are simulated, 80ms for MS configurations and 400ms for LS configurations. If the physical time to simulate increases with the size of the configuration, this is also the case for the time step which is here controlled by convection (the

acoustic CFL number is 0.7 at all scales): it increases from about 0.05μs at SS to 0.3μs at MS and 1.4μs at LS. As a consequence, since the computational grids are comparable (20 millions cells), the computation cost for one LES is almost constant for all configurations, SS, MS or LS: about 100 000 core-hours for an elapsed time of 24 hours.
To verify mesh independency for the SS case, an additional LES called VRLES (Very Refined LES) was performed on 131 072 processors of the BlueGene/Q machine Mira from ALCF (INCITE award) using a finer mesh of 973 million cells (Section 4.3).

4. LES of the small-scale experiment

Note that some of the small-scale LES presented hereafter have been already mentioned in [69]. However, for the sake of clarity and exhaustiveness, the full set of small-scale results is presented here.

4.1. Base case: BBBS configuration, C_3H_8

Figure 7 shows LES images of flame propagation compared with experiments in the SS case [28]. Only the LES performed with the efficiency function of Colin *et al.* is shown here but the results are qualitatively similar with the efficiency function of Charlette *et al.* In the early stage of propagation, the flame is laminar and hemispherical. At $t - \Delta t_{peak}$=6ms, it hits the first baffle plate passing first through the two central passages and then through the lateral passages. The four finger-shaped flames merge together before reaching the second baffle plate ($t - \Delta t_{peak}$=8ms). At that point, the flame is still almost laminar since the turbulence generated in the wake of the first obstacle is very low. When touching the second baffle plate, the flame starts accelerating ($t - \Delta t_{peak}$=9.6ms). Four fingers are formed again but this time, they begin to be wrinkled by the higher turbulence level encountered behind the obstacle ($t - \Delta t_{peak}$=10ms). Between the second and third obstacles, due to the higher flame front speed, there is not enough time for the different fingers to merge again. They finally hit the third

baffle plate and the central obstacle ($t - \Delta t_{peak}$=10.8ms), while continuing to accelerate. All these phases are well reproduced by LES.

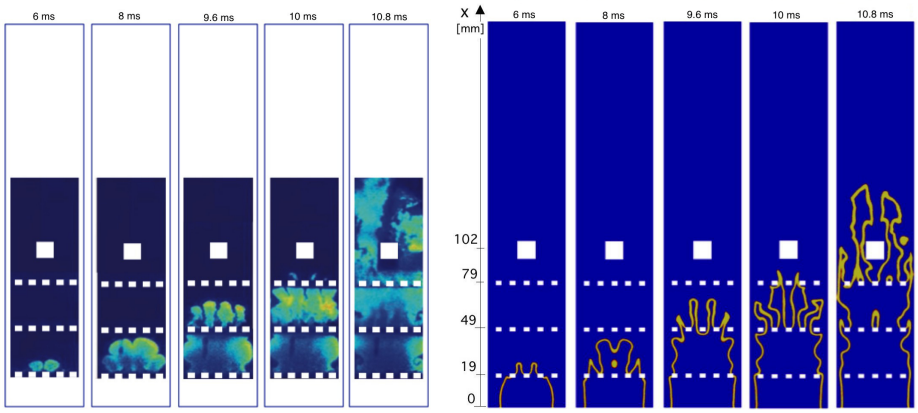

Figure 7: Flame propagation in the configuration BBBS SS (C_3H_8, Φ=1). **Left**: Time sequence of LIF-OH images [28]. **Right**: Time sequence extracted from the LES (visualization of the reaction rate). The corresponding physical times $t - \Delta t_{peak}$ are given at the top of each image.

The evolution of the speed of the leading point of the flame as a function of its position is shown in Fig. 8 (left). Indications of the corresponding physical time $t - \Delta t_{peak}$ are also provided to compare with overpressure-time traces shown afterwards (Fig. 12). This speed is controlled by dilatation and by the turbulent combustion model. The LES performed with the model of Colin *et al.* reproduces perfectly the different phases of propagation and the successive flame accelerations (especially around the second baffle plate) and decelerations (mainly between the second and third baffle plates). Some discrepancies are observed downstream of the central obstacle but this may be partly due to the limited resolution of high-speed images. In this area and considering the high flame speed, the position of the flame front can only be reported every 2 centimeters, which is not enough to obtain an accurate estimate of its speed. At the peak pressure instant $t - \Delta t_{peak}$=11.44ms, the leading point of the flame front is already far downstream of the central obstacle but the main part of the

reaction rate is still located around the obstacle.

With the model of Charlette *et al.*, the LES matches the experiments up to the second baffle plate. From the third baffle plate, it starts overestimating the flame front speed. This may be directly attributed to the modeling of the sub-grid

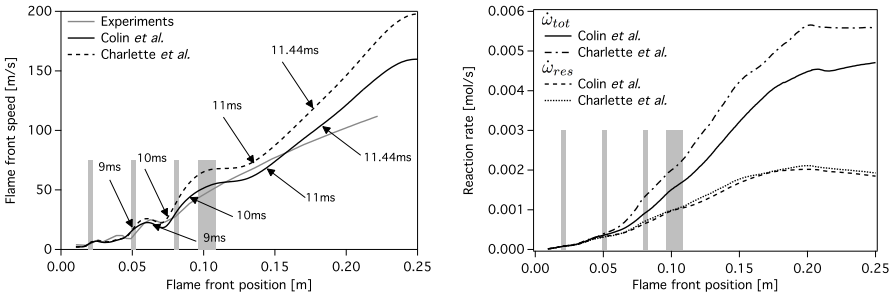

Figure 8: LES of the configuration BBBS SS (C_3H_8, Φ=1) with the models of Colin *et al.* and Charlette *et al.* **Left**: evolution of the flame front speed as a function of the flame front position. Black arrows shows the corresponding physical time $t - \Delta t_{peak}$ (note that Δt_{peak} is different for each LES as explained in Section 2.2). **Right**: total ($\dot{\omega}_{tot}$) and resolved ($\dot{\omega}_{res}$) reaction rates.

scale wrinkling, as confirmed by Fig. 8 (right) which compares the reaction rates (total $\dot{\omega}_{tot}$, resolved $\dot{\omega}_{res}$ and consequently sub-grid scale $\dot{\omega}_{sgs} = \dot{\omega}_{tot} - \dot{\omega}_{res}$) obtained with the Colin *et al.* and Charlette *et al.* models. The total reaction rates of both models follow exactly the same trends as for the flame front speed: equal up to the second baffle plate and very different from the third baffle plate. For both LES, the resolved reaction rates are almost the same during the whole computation, revealing a low impact of the sub-grid scale modeling on the resolved scales. However, the sub-grid scale modeling itself strongly affects the results, especially from the third baffle plate. When the flame interacts with the central obstacle, the sub-grid scale reaction rate contributes between 30% and 50% to the total reaction rate and up to 70% downstream of the central obstacle. This highlights the great importance of the sub-grid-scale combustion model for these simulations, as shown by Di Sarli *et al.* [70, 71].

Figure 9 displays a field of efficiency function $\mathcal{E}$ (Eq. 1) obtained with the two

models for the same location of the flame front, when the flame interacts with the central obstacle. At these location and time, turbulence levels are high and the range of $\mathcal{E}$ values observed are representative of the maximum values obtained in the LES. Whatever the model used, the efficiency function activates in the same locations, mainly around the central obstacle, around and in the wake of the second and third baffle plates. But the levels of efficiency factors may be locally very different: if they are relatively similar around the central obstacle, this is no longer the case upstream of it, where the model of Charlette *et al.* predicts much higher levels. This is confirmed by Figs. 10 and 11, which show the scatter plot of the efficiency function as a function of the sub-grid scale turbulent velocity u'_Δ and the probability density function of $\mathcal{E}$ respectively. The analytical functions (using Eqs. 2 and 3) are also superimposed to the scatter plots. The model of Colin *et al.* exhibits a large range of efficiency, uniformly distributed over the turbulence intensity while the model of Charlette *et al.* exhibits a strong peak around 3 due to the "bending effect" incorporated in its formulation at high u'_Δ/S_l^0 [48]. The scatter plot dispersion around the analytical expressions (Eqs. 2 and 3) is due to the non exactly uniform mesh size. Overall, the model of Charlette *et al.* generates higher values of the efficiency function except for very high turbulence levels ($u'_\Delta > 12.5\ m.s^{-1}$). Consequently, it also predicts higher reaction rates and flame speeds than the model of Colin *et al.*, from the beginning of the turbulent propagation phase (i.e. between the second and third baffle plates).

The resulting overpressure-time traces (measured in the base plate) are plotted in Fig. 12. For the experimental data, the trace represents the envelope of the different realizations. The model of Charlette *et al.* predicts higher levels of overpressure than the model of Colin *et al.* and overestimates the experimental peak value (173 mbar instead of 113 mbar). With the model of Colin *et al.*, the rate of pressure rise, the peak pressure and the postpeak phase are correctly described. The pressure oscillations observed after 12 ms at a frequency of about 650 Hz correspond to the excitation of the first longitudinal acoustic mode of the

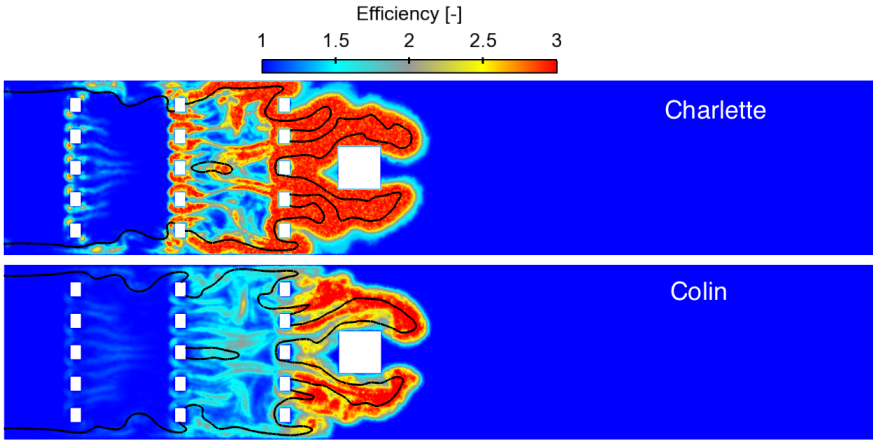

Figure 9: Field of efficiency function (Eq. 1) with the Colin *et al.* (bottom) and Charlette *et al.* (top) models and isoline of temperature $T = 1500K$ (black line) when the flame interacts with the central obstacle (same location of the flame front). Configuration BBBS SS (C_3H_8, Φ=1).

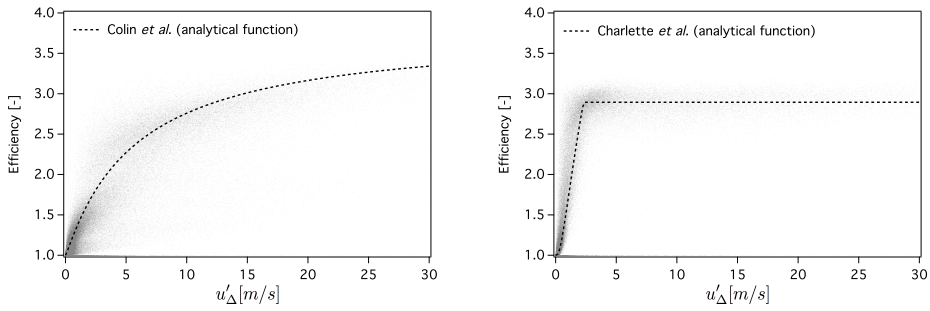

Figure 10: Scatter plot of the efficiency function $\mathcal{E}$ as a function of the sub-grid scale turbulent velocity u'_Δ for the models of Colin *et al.* (**left**) and Charlette *et al.* (**right**). The analytical functions Eqs. 2 and 3 are also plotted using a constant $\Delta = 0.5$mm. Data are extracted from the snapshots displayed in Fig. 9. Configuration BBBS SS (C_3H_8, Φ=1).

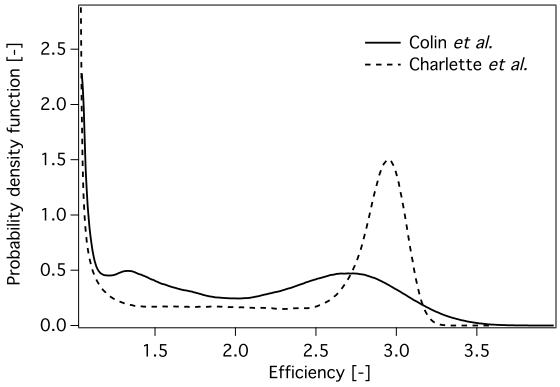

Figure 11: Probability density function of the efficiency function $\mathcal{E}$ for the models of Colin *et al.* and Charlette *et al.* Data are extracted from the snapshots displayed in Fig. 9. Configuration BBBS SS (C_3H_8, Φ=1).

duct (considering a non zero impedance at its exit) and are perfectly captured by LES [51].

This shows that the model of Colin *et al.* is well suited for describing the whole explosion transient. Even the laminar to turbulent transition phase is correctly captured despite the underlying equilibrium assumption on which it is based. However, this result is highly dependent on the value of the model constant β_{Colin}. Figure 13 (left) shows the overpressure for three different values of β_{Colin} (0.1, 0.3 (standard value) and 1.0). Higher β_{Colin} values lead to faster flame propagation and higher overpressure. For $\beta_{Colin} = 1.0$, the maximum overpressure is about 185 mbar while it is about 113 mbar for $\beta_{Colin} = 0.3$ and only 67 mbar for $\beta_{Colin} = 0.1$. The same conclusion holds for the model of Charlette *et al.* (Fig. 13 (right)): if a constant $\beta_{Charlette} = 0.4$ is used instead of the original value 0.5, the prediction of the overpressure is greatly improved and matches almost perfectly the result obtained with the model of Colin *et al.* with $\beta_{Colin} = 0.3$. This shows that both models are able to reproduce the experimental behavior, although their formulations are sensibly different. But this also shows that the choice of the constant for this kind of algebraic closure remains a major challenge. The recent development of dynamic

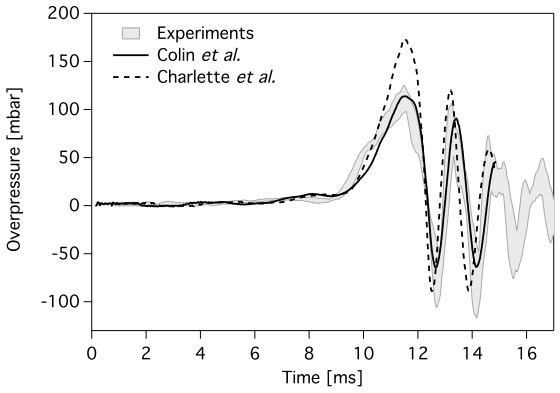

Figure 12: Pressure-time traces for configuration BBBS SS (C_3H_8, Φ=1). Comparison between experiments (envelope) and LES performed with the models of Colin *et al.* and Charlette *et al.*

models [72, 20], theoretically able to automatically adjust the model parameters during the simulation, could be a promising way-out to solve this issue in the future.

For the following parametric variations, only the results obtained with the model of Colin *et al.* will be shown and discussed.

4.2. Parametric variations

The effect of different parametric variations are now studied:

- effect of the number of obstacles;
- effect of the location of the obstacles;
- effect of the type of fuel.

The objective is to check if the numerical setup used in Section 4.1 to simulate the BBBS - C_3H_8 case is able to handle the different configurations described in Table 1 without any adjustment. All numerical models and parameters are kept unchanged, except the laminar flame thickness and the laminar flame speed

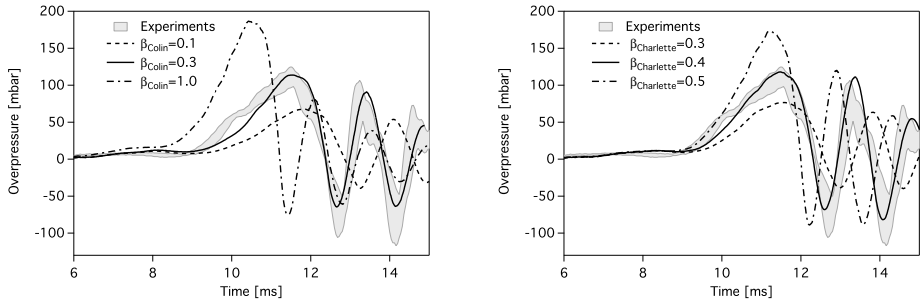

Figure 13: Pressure-time traces for configuration BBBS SS (C_3H_8, Φ=1). Comparison between LES performed with the models of Colin *et al.* (**left**) and Charlette *et al.* (**right**) for different values of the model constant (β_{Colin} =0.1, 0.3 or 1.0; $\beta_{Charlette}$ =0.3, 0.4 or 0.5). To illustrate the differences in propagation speed, LES traces are not shifted in time individually but by a same quantity using the peak pressure instant t_{peak}^{LES} obtained with β_{Colin} =0.3 and $\beta_{Charlette}$ =0.4 for the left and right figures respectively.

required to calculate the thickening factor and the efficiency function, which are adapted to the considered mixture (C_3H_8, CH_4 or H_2) as mentioned in Section 3.

The effect of the number of baffle plates is shown in Fig. 14. LES overpressure time traces are compared to the experimental results for three configurations with 1, 2 or 3 baffle plates respectively, the fuel being C_3H_8. LES reproduces the overpressure magnitude for any of the three configurations: the flame is accelerated when adding obstacles, and the resulting overpressure is higher. As already mentioned by Masri *et al.* [28], this result is mainly due to an increasing global level of turbulence in the chamber as the number of obstacles increases. Postpeak oscillations are correctly captured as well. The effect of the position of the obstacles is also well captured by LES (Fig. 15). For this comparison, only one baffle is used, in first (configuration BOOS) or third position (configuration OOBS). These two configurations are very different since OOBS shows extensive wrinkling after the baffle plate and around the central obstacle while in BOOS, the flame front is quasi laminar all along the channel. Indeed for configuration BOOS, the slight turbulence introduced by the first baffle is totally dissipated before the flame reaches the central obstacle. Figure 15 thus confirms that, as

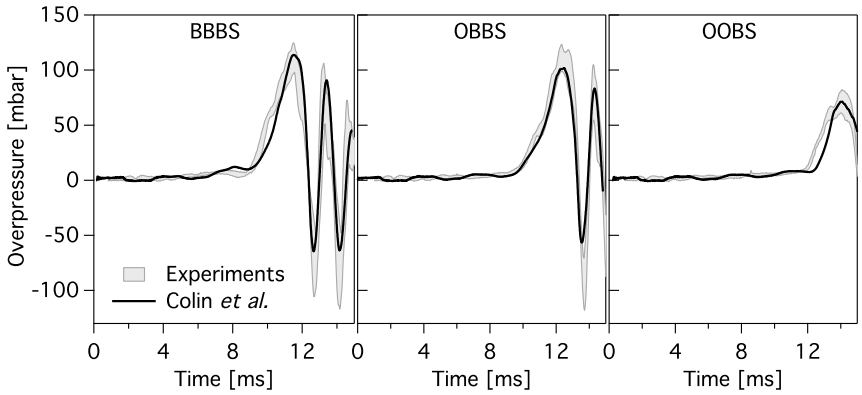

Figure 14: Comparison of overpressure signals between LES (efficiency model of Colin *et al.*) and experiments (envelope) when changing the number of baffle plates (SS, C_3H_8, Φ=1).

expected, the model of Colin *et al.* is able to correctly degenerate towards a laminar behavior in the absence of turbulence. Figure 16 highlights the fuel influence for different explosions performed in configuration BBBS. H_2 explosions generate the highest overpressures (and the highest flame front speeds, not shown here), followed by C_3H_8 and CH_4 explosions, as expected from their respective flame speeds: $S_l^0(H_2, \Phi = 0.7) = 128\ cm.s^{-1} > S_l^0(C_3H_8, \Phi = 1) = 38.4\ cm.s^{-1} > S_l^0(CH_4, \Phi = 1) = 36.3\ cm.s^{-1}$. Even though LES correctly reproduces this global trend, it significantly underestimates the overpressure for H_2. In this case, the overpressure peak is significative (about 0.8 bar in the experiments) and the assumption that the laminar flame thickness remains constant during the whole computation (see Section 3) is incorrect. Indeed, if the pressure increases from 1 bar to 1.8 bar, it means that the flame thickness should in fact decrease to 40% when compared to atmospheric conditions, causing the flame to be locally under resolved. Even if this issue is limited to a relatively short duration compared to the total duration of the explosion, the underestimation of the thickening and efficiency factors (Eqs. 2 and 3) may be a reason for the lower overpressure obtained in the LES. One possible approach to address this problem in the future is to introduce a pressure-dependent flame

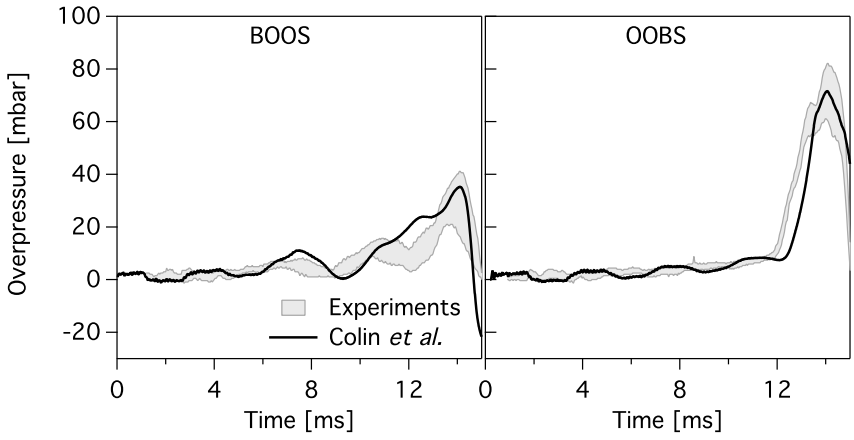

Figure 15: Comparison of overpressure signals between LES (efficiency model of Colin *et al.*) and experiments (envelope) when changing the position of the baffle plate (SS, C_3H_8, Φ=1).

thickness in the expression of the efficiency function in order to get a pressure-dependent thickening.

To conclude with the SS results, LES performed with the model of Colin *et al.* is able to reproduce the whole transient of an explosion scenario for all configurations and fuels. This was in some ways unexpected since this kind of algebraic closure is *a priori* not tailored to handle out-of-equilibrium situations such as laminar-turbulent and turbulent-laminar transitions. However, as mentioned in the introduction, the range of variations in terms of Reynolds and Damköhler numbers is narrow in this case and larger parametric variations are desirable to assess the behavior of the model. This will be the subject of Section 5 thanks to the MS and LS cases.

4.3. Mesh dependency

The previous section has shown the dependence of the results on the turbulent combustion model. At this point, an important question is mesh dependency [73, 74]. This issue is all the more important for the following since the

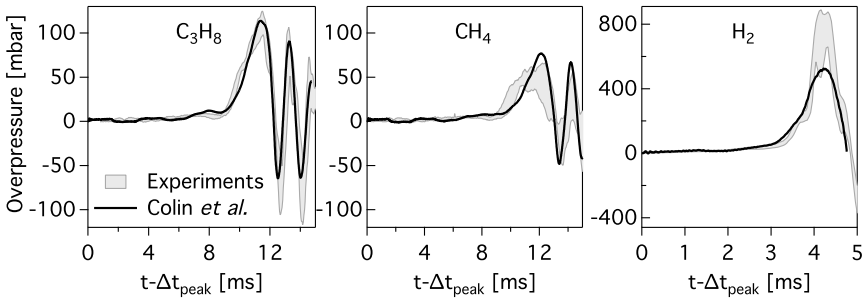

Figure 16: Comparison of overpressure signals between LES (efficiency model of Colin *et al.* and experiments (envelope) when changing the type of fuel (CH_4: Φ=1; C_3H_8: Φ=1; H_2: Φ=0.7). Configuration BBBS SS.

grid resolutions used in the SS configuration and in the MS and LS configurations differ significantly (0.5, 3 and 12.2 mm respectively in the refined region). In order to assess the quality of the LES and in particular its dependency to the grid resolution, a VRLES was performed and compared to the LES presented in the last section. Configuration OOBS is considered here. This configuration induces a weakly turbulent flow for which the requirements in terms of mesh resolution are expected to be much lower than for the base case BBBS for instance. The efficiency function of Colin *et al.* is used in both cases. The key features of this VRLES are summarized in Table 5 in terms of number of cells and characteristic length scales: on this very fine grid, the level of description of the simulation corresponds to a Quasi-Direct Numerical Simulation (QDNS) of the flame. The LES models described above are always activated during the simulation. They naturally degenerate towards DNS if the mesh resolution is high enough. Verifying that their contribution in this QDNS case remains very low is a good way to estimate the quality of the simulation. The objectives of this comparison are thus manyfold:

- assess the LES dependency to the grid resolution;
- check that LES naturally tends towards DNS when the resolution is high

	LES	VRLES
Number of cells	20.10^6	973.10^6
$\mathbf{\Delta_x}$ $[mm]$	0.500	0.136
$\mathbf{l_t/\Delta_x}$ [-]	11.6	42.6
$\eta_\mathbf{k}/\mathbf{\Delta_x}$ [-]	0.07	0.26
$\delta_\mathbf{L}^\mathbf{0}/\mathbf{\Delta_x}$ [-]	0.68	2.5
CPU cost [core-hours]	1.10^5	25.10^6

Table 5: Grid characteristics for the VRLES and the LES of the OOBS SS configuration. Δ_x is the grid size, δ_l^0 is the laminar flame thickness, l_t and η_k are estimates of the integral and Kolmogorov length scale respectively. All simulations were performed on BlueGene/Q machines.

enough;

- thanks to this numerical experiment, provide a comprehensive database which may be used thereafter to help developing and validating models.

Figures 17 and 18 reveal very similar flame structures with LES and VRLES at five successive times. Of course VRLES exhibits many more turbulent structures, from the laminar propagation phase (top images) where vortex shedding behind the baffle plate is clearly evidenced to the fully turbulent propagation phase (bottom images) where the flame is much more wrinkled and distorted. But it confirms that the 20 million grid combined with the sub-grid models is able to capture the main features of the explosion. In particular the flame passage through the baffle plate and around the central obstacle in LES and VRLES is fully comparable. The bottom images show that a lot of turbulent structures are still present well after the central obstacles (the right border of the figure corresponds to x≈20cm). This turbulence supports the flame development even if there are no further obstacles downstream of the central obstacle. It explains why the flame still accelerates until the end of the explosion chamber, as shown in Fig. 19 (left) which compares the LES and VRLES flame front speeds. This figure shows that the LES and VRLES flames propagate in a very similar

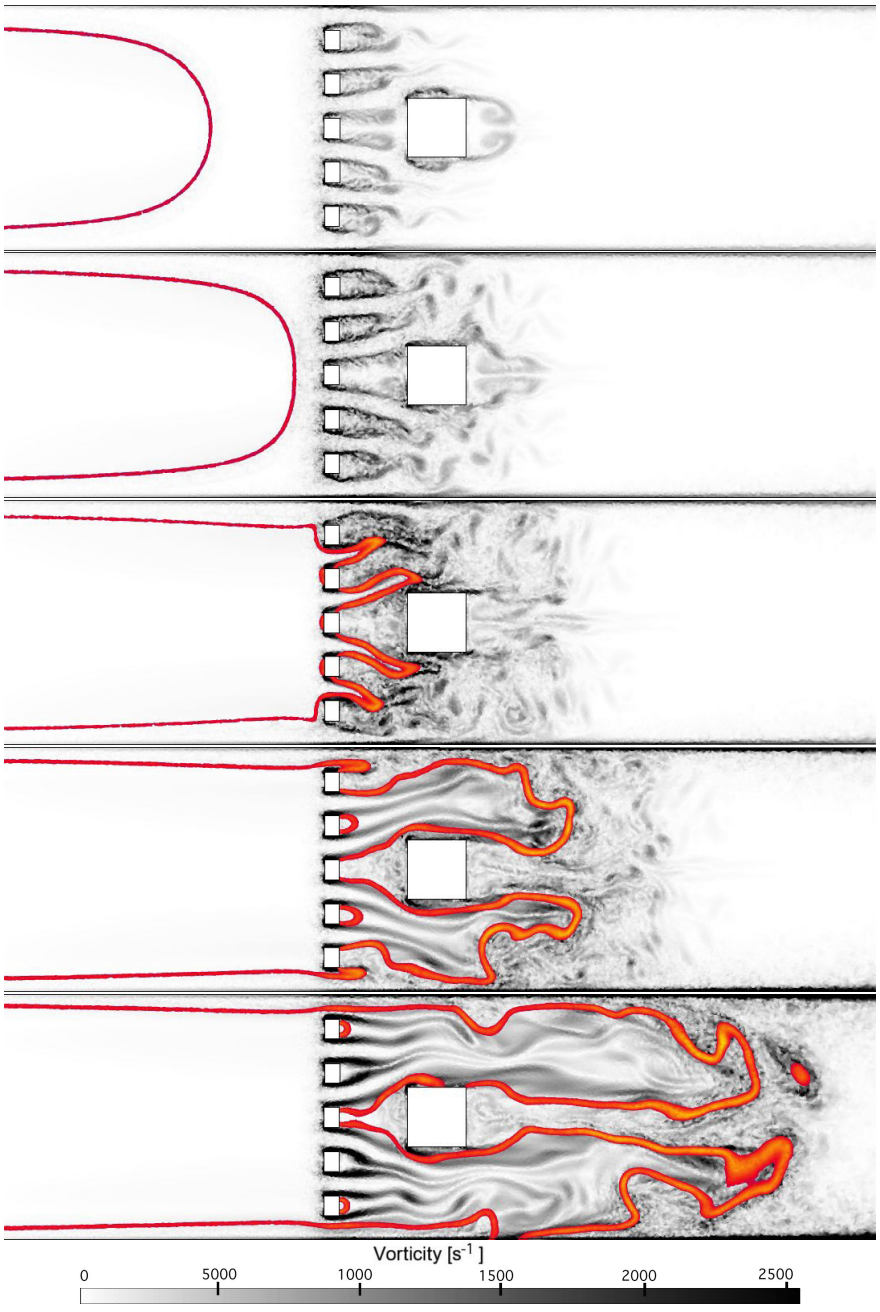

Figure 17: LES (20.10^6 cells, Δ_x=0.5 mm) of flame propagation in configuration OOBS SS (C_3H_8, Φ=1). Time sequence at $t - \Delta t_{peak}$=9.3, 10.8, 11.9, 12.8 and 13.5 ms (from top to bottom). Vorticity field and isoline of heat release.

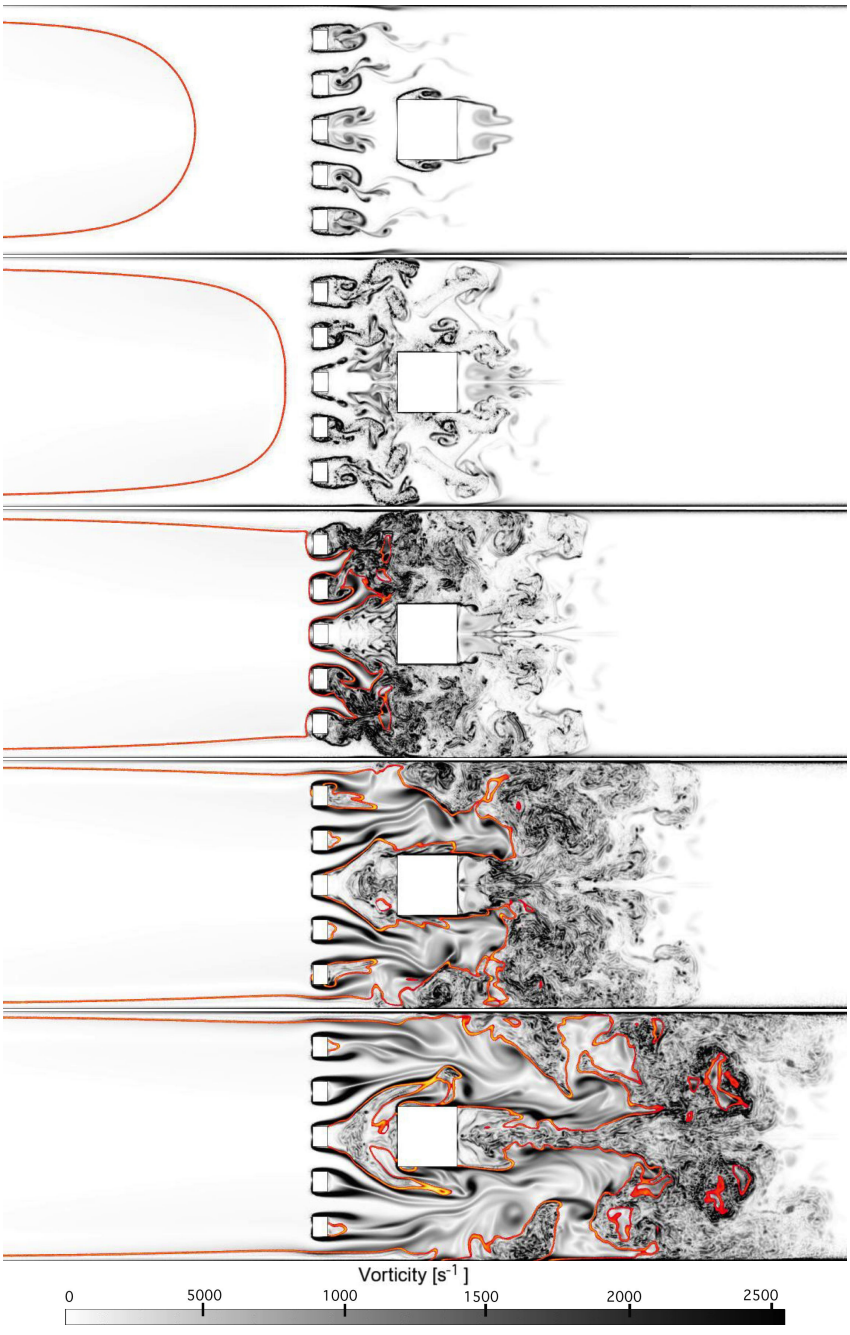

Figure 18: VRLES (973.10^6 cells, Δ_x=0.136 mm) of flame propagation in configuration OOBS SS (C_3H_8, Φ=1). Time sequence at $t - \Delta t_{peak}$=9.3, 10.8, 11.9, 12.8 and 13.5 ms (from top to bottom). Vorticity field and isoline of heat release.

way. With VRLES the accelerations and decelerations around the obstacles are slightly more pronounced but this is mainly a post processing artefact due to small pockets of burnt gases detaching from the main flame front under the action of small vortices (the flame front position is here defined as the leading point where T>1500K). This is confirmed by Fig. 19 (right) which shows that overpressure signals obtained with LES and VRLES overlap almost perfectly.

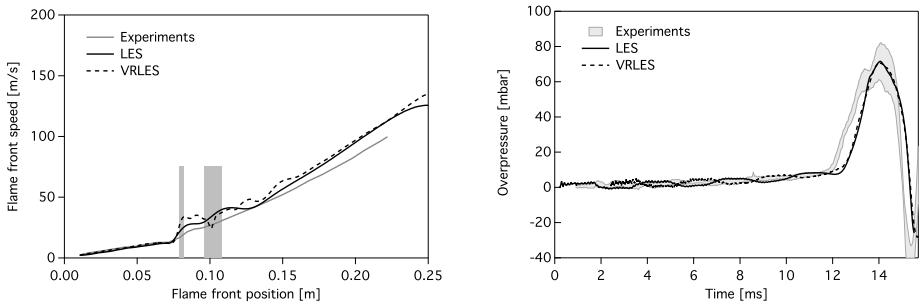

Figure 19: Comparison between VRLES and LES with the model of Colin *et al.* for configuration OOBS SS (C_3H_8, Φ=1). **Left**: evolution of the flame front speed as a function of the flame front position. **Right**: Pressure-time traces.

Finally, the evolution of the total and resolved reaction rates for the LES and VRLES (Fig. 20) confirms that the designation VRLES or even QDNS (for the flame) is appropriate since the reaction rate is almost totally resolved in this simulation. The sub-grid scale reaction rate remains very low all along the computation, with a contribution which does not exceed 8% of the total reaction rate in the refined zone, i.e. for $x < 16$cm. This also illustrates the correct behavior of the LES combustion model which goes to DNS as expected when the flame resolution is sufficient. For the LES, the sub-grid scale model contributes up to 35% of the total reaction rate at the end of the refined zone ($x = 16$ cm) and around 23% at the central obstacle location ($x \approx 10$ cm). The two total reaction rate curves match almost perfectly, confirming the grid independency of the results.

5. LES of the medium-scale and large-scale experiments

When going from the SS configuration to the MS and to the LS configurations, the geometry is scaled by a factor 6 and 24.4 respectively. It means that the integral length scale l_t increases by roughly the same factor. Since we have chosen to work at constant numerical cost whatever the configuration (similar meshes with about 20 millions cells at SS, MS and LS), the grid size Δ_x also

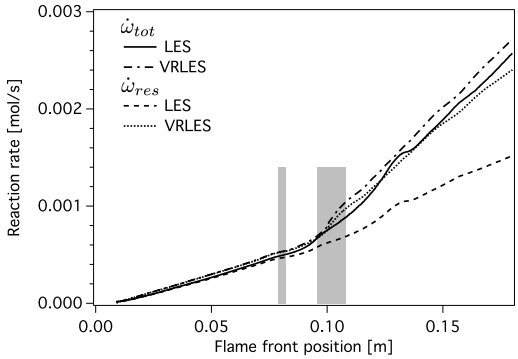

Figure 20: Comparison between VRLES and LES with the models of Colin *et al.* for configuration OOBS SS (C_3H_8, Φ=1): total ($\dot{\omega}_{tot}$) and resolved ($\dot{\omega}_{res}$) reaction rates.

scales by the same factor. Considering an idealized turbulence (homogeneous isotropic turbulence), the ratio of the integral length scale to the Kolmogorov length scale η_k, may be expressed as $\frac{l_t}{\eta_k} \sim Re_t^{3/4}$. The velocity scale appearing in this turbulent Reynolds number is very difficult to estimate accurately. As a rough estimate, it may be considered as proportional to the laminar flame speed since it is the velocity field created by the laminar flame which induces turbulence. The Kolmogorov scale η_k may thus be written as $\eta_k \sim \left(\frac{\nu}{S_l^0}\right)^{3/4} {l_t}^{1/4}$. Finally, the characteristic length scale for combustion, i.e. the laminar flame thickness δ_l^0, may be considered as constant as a first approximation, neglecting the influence of the overpressure generated during the explosion. The evolution of these characteristic length scales is plotted in Fig. 21. It shows that the smallest and largest turbulence length scales are not equally upscaled with the grid size. Since the smallest length scales increase more slowly than the largest scales and the grid size, the proportion of turbulent sub-grid scales is expected to increase from SS to LS. This is even more true for combustion since the laminar flame thickness does not increase with the size of the configuration. As a consequence, the contribution of the turbulent combustion model is expected to increase even more when going from SS to MS and to LS. It means that even if all numerical models and parameters are kept constant at all scales, the

behavior of the efficiency function will become crucial when the scale of the configuration increases. Note also that the non-dependence of the thickening to the pressure, as discussed in Section 4.2, introduces an additional modeling uncertainty at medium and large-scales due to the larger levels of overpressure reached in these configurations.

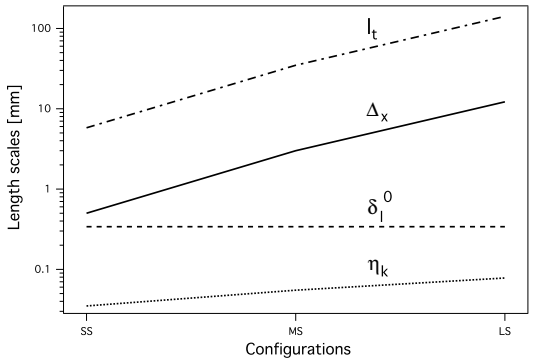

Figure 21: Evolution of the characteristic length scales l_t, η_k, δ_l^0 and Δ_x when going from SS to LS (for a given fuel and mixture composition).

5.1. Medium-scale experiment

As for the SS experiment, the behavior of the models of Colin *et al.* and Charlette *et al.* is first assessed on the base case of the MS setup, i.e. configuration BBBS with C_3H_8. The propagation of the flame is illustrated in Fig. 22. Experimental images are extracted from a high-speed video and the LES ones are taken from the Charlette *et al.* computation (similar flame structures are observed with the model of Colin *et al.* but not shown here). Contrary to the SS experiment, the MS images of Fig. 22 are side views that do not allow a clear visualization of the flame front shape. In particular the finger-shaped flames which emerge from the baffle plates are not visible in this case. Nonetheless, they allow a first qualitative comparison of the flame propagation. The LES flame and the experimental flame proceed globally at the same speed and in the

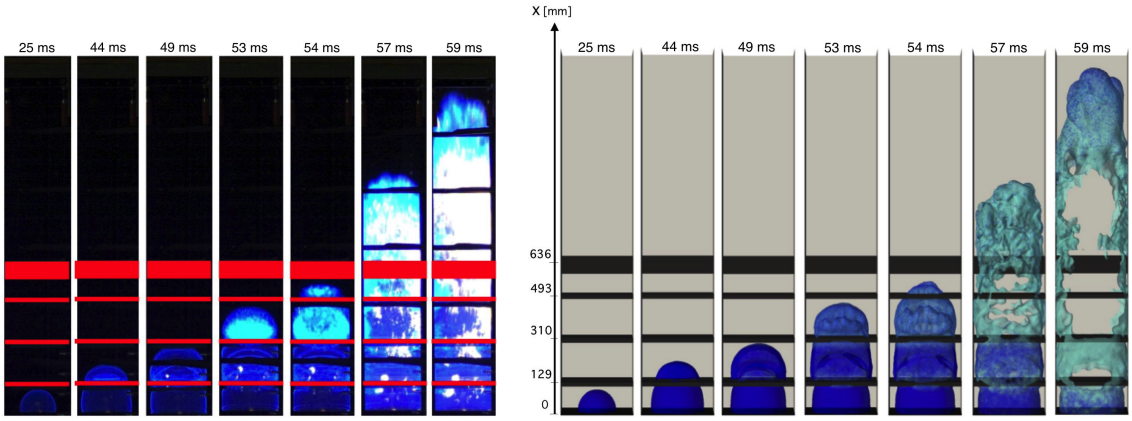

Figure 22: Flame propagation in configuration BBBS MS (C_3H_8, Φ=1). **Left**: Time sequence of high-speed experimental images. **Right**: Time sequence extracted from the LES (visualization of the reaction rate). The corresponding physical times $t - \Delta t_{peak}$ are given at the top of each image.

same way. As for the SS case, the flame remains laminar after the first baffle plate and begins to wrinkle after having passed through the second baffle plate. The overall propagation is much longer in the MS case, with about 28 ms to go from the first to the third baffle compared to about 4 ms in the SS case.

The evolution of the flame front speed (Fig. 23 left) reveals an explosion scenario which is very similar to the SS case, with successive accelerations and decelerations as the flame progresses through the channel alongside the obstacles. Both models reproduce this behavior but with varying degrees of success: the model of Charlette *et al.* matches very well the experimental results while the model of Colin *et al.* largely underestimates them from the second baffle plate. Downstream of the obstacles, the flame front speed exceeds 350 $m.s^{-1}$ in the experiments and with the model of Charlette *et al.* whereas it hardly reaches 275 $m.s^{-1}$ with the model of Colin *et al.* These predictions are the direct consequence of the sub-grid scale combustion modeling: Fig. 23 (right) shows that, when the flame reaches the central obstacle, the sub-grid scale contribution is

approximately 80% of the total reaction rate with the model of Charlette *et al.* (50% in the SS case) and about 60% with the model of Colin *et al.* (30% in the SS case). As previously, the sub-grid scale modeling does not significantly impact the resolved reaction rate, which means that the global reaction rate and the resulting flame speed are directly proportional to the sub-grid scale contribution. As expected since the overpressure generated in the chamber is

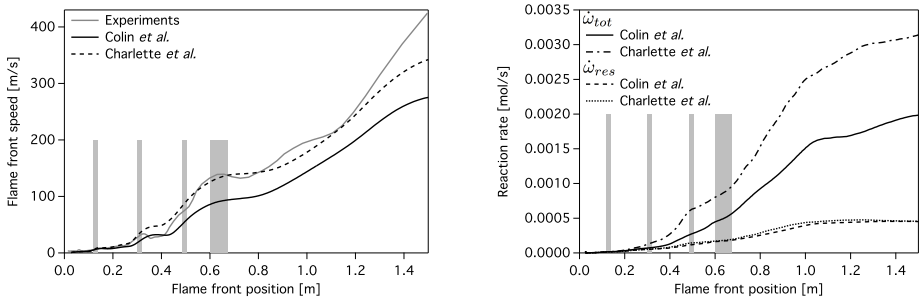

Figure 23: LES of the configuration BBBS MS (C_3H_8, Φ=1) with the models of Colin *et al.* and Charlette *et al.* **Left**: evolution of the flame front speed as a function of the flame front position. **Right**: total ($\dot{\omega}_{tot}$) and resolved ($\dot{\omega}_{res}$) reaction rates.

strongly linked to the flame front speed, Fig. 24 (left) shows that the LES with the model of Colin *et al.* underestimates the peak pressure while the model of Charlette *et al.* predicts it remarkably well. Figure 24 (right) gives additional details for the model of Charlette *et al.*, showing the spatial distribution of the overpressure for the seven instants displayed in Fig. 22. Since the pressure is almost homogeneous in the Y and Z directions, only profiles along the longitudinal direction X are plotted.

The conclusion reached here for the MS case is opposite compared to the SS configuration: the Charlette *et al.* model seems to perform better than the Colin *et al.* model. This highlights the limited predictive capacities of this kind of constant-coefficients sub-grid scale modeling. Of course, this does not mean that the model of Charlette *et al.* is better suited for MS configurations or that the model of Colin *et al.* is unadapted for larger size cases. It simply shows

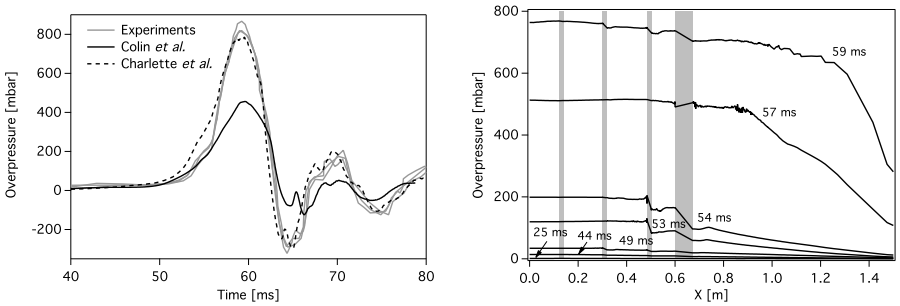

Figure 24: Configuration BBBS MS (C_3H_8, Φ=1). **Left**: pressure-time traces, comparison between experiments (three realizations) and LES performed with the models of Colin *et al.* and Charlette *et al.* **Right**: model of Charlette *et al.*, overpressure distribution in the center of the combustion chamber (Y=0, Z=0) and along the longitudinal direction X for the seven instants $t - \Delta t_{peak}$ displayed in Fig. 22.

that the scales and flow conditions in the MS case diverge too widely from the SS case to allow a unique fixed-constant model to behave well over such a range of variations and that the SS - MS cases constitute a challenging test case for turbulent combustion sub-grid scale models. For the following tests, the model of Charlette *et al.* with $\beta_{Charlette} = 0.5$ is retained since it provides the better predictions on the MS base case.

The influence of fuel type on the overpressure is shown in Fig. 25. As for the SS experiment, stronger overpressure magnitudes are obtained with C_3H_8 compared to CH_4. LES performed with the model of Charlette *et al.* match experimental results with an approximate 35% reduction in peak pressure when going from C_3H_8 to CH_4. Figure 26 illustrates the effect of the number of grids comparing configurations BBBS and OOBS. Results are similar to the ones obtained in the SS experiments. The flame propagation (not shown) is similar in both configurations up to the second obstacle position since the turbulence induced by the first baffle in the BBBS case is very weak. From the second obstacle position, the flame strongly accelerates in configuration BBBS whereas it remains laminar in configuration OOBS. The final flame speed down-

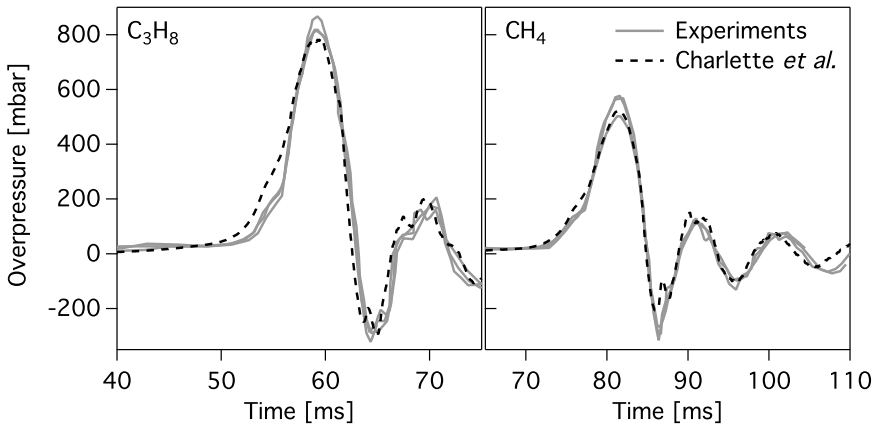

Figure 25: Comparison of overpressure signals between LES (efficiency model of Charlette *et al.*) and experiments (three realizations) when changing the type of fuel (configuration BBBS MS).

stream of the central obstacle hardly reaches 275 $m.s^{-1}$ in configuration OOBS in comparison with the 350 $m.s^{-1}$ attained in the BBBS configuration. The resulting overpressure traces show a larger peak pressure in the BBBS configuration (about 800 mbar) compared to the OOBS configuration (about 540 mbar). Once again, LES captures the peak magnitude and postpeak transient.

5.2. Large-scale experiment

As mentioned in Section 2.2, no images of the flame propagation are available for the large-scale experiment. The overpressure generated in the chamber is thus the only material available here for comparison. For the sake of concision and since the same kind of agreement between LES and experiments is obtained at LS compared to MS, only the maximum pressure peak is reported in the following figures. More precisely, since shot-to-shot variations are more important in this LS rig compared to the MS rig, both minimum and maximum experimental values of the maximum pressure peak will be compared to LES. Note that the LES flame does not propagate much faster than in the corresponding MS

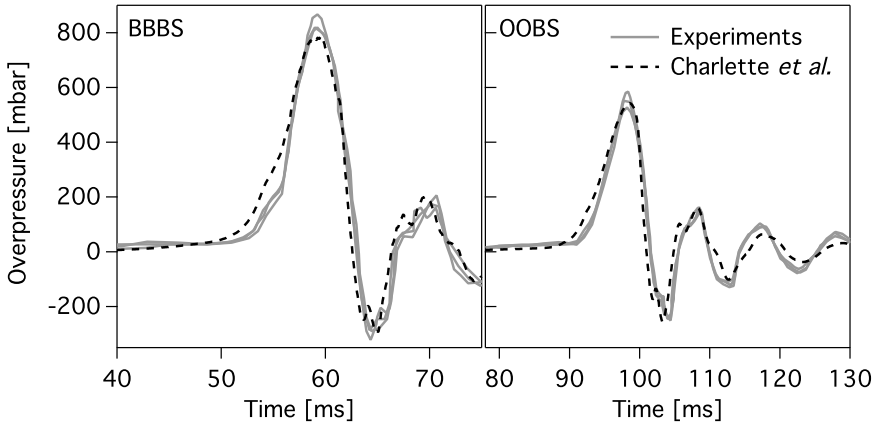

Figure 26: Comparison of overpressure signals between LES (efficiency model of Charlette *et al.*) and experiments (three realizations) when changing the number of baffle plates (MS, C_3H_8, Φ=1).

configurations (about 400 m/s downstream of the central obstacle versus 350 m/s for configuration BBBS for instance) and does not transition to detonation.

Focusing first on the base case BBBS, the predictions of the models of Colin *et al.* and Charlette *et al.* are compared in Fig. 27. As for the MS case, the overpressure is strongly underestimated with the model of Colin *et al.* while it is fairly well predicted with the model of Charlette *et al.* For this BBBS LS case, the magnitude of the overpressure is about 1620 mbar (in the LES), compared to about 800 mbar for the MS configuration (ratio 2.0) and 110 mbar for the SS configuration (ratio 14.7) with the same arrangement of baffle plates. Once again, the pressure transient is also well described by LES (not shown). For the following configurations, only the model of Charlette *et al.* is considered.

Parametric variations for the LS experiment focused on the fuel type (C_3H_8 versus CH_4) and the number of grids (one for configuration OOBS and three for configuration BBBS). Figure 27 (right) shows the influence of the number

of baffle plates: as for the SS and MS cases, LES correctly predicts the increase of pressure when adding obstacles. The ratio between the peak pressures obtained in the three baffles configuration and in the single baffle configuration is approximately 1.2, which is much lower than in the MS case (ratio 1.5) and SS case (1.55). The comparison between LES and experiments when changing the type of fuel is displayed in Fig. 27 (left). The larger flame speed obtained using C_3H_8 compared to CH_4 leads to a stronger peak pressure with C_3H_8, as at smaller scales. The ratio between the peak pressures obtained using C_3H_8 and CH_4 is about 1.2 for the LS case, 1.5 for the MS case and 1.8 for the SS case. These observations show that globally the SS configurations are the most sensitive to parametric variations (geometric or physical). This also illustrates

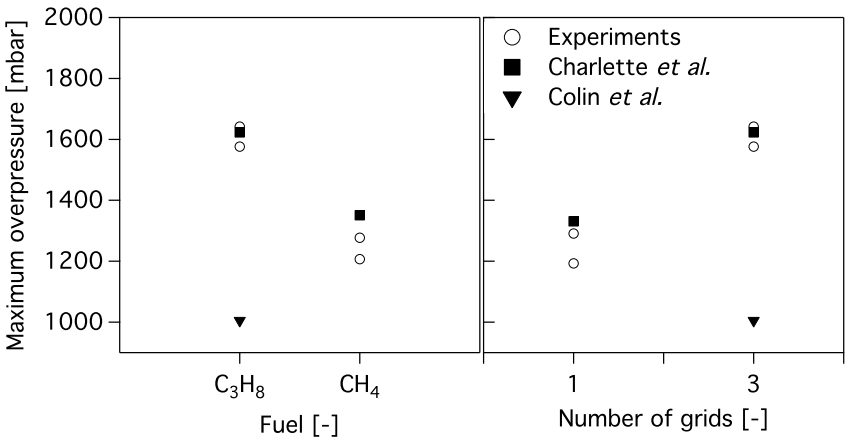

Figure 27: Comparaison between LS experiments (minimum and maximum values over the different experimental realizations) and LES performed with the models of Colin *et al.* and Charlette *et al.* **Left**: Influence of the type of fuel. **Right**: influence of the number of baffle plates.

that upscaling effects are highly non linear and trying to extrapolate the characteristic parameters of an explosion, typically the overpressure, using simple scaling laws is far from obvious.

6. Conclusions

A new experimental database has been presented to study upscaling effects in a vented explosion configuration and more generally the performances of premixed turbulent combustion models. This database which uses three venting chambers, the original Sydney setup [28] and two Gexcon replicas scaled by 6 and 24.4, allows to test and validate different numerical approaches and models over a wide range of turbulent combustion regimes, with unambiguous initial and boundary conditions. Mesh dependency was tested using a highly resolved quasi-DNS simulation (1 billion points). It is also a difficult test where flames can alternate between laminar and turbulent regimes.

Two LES sub-grid scale combustion models (the algebraic models of Colin *et al.* and Charlette *et al.*) were compared in terms of flame propagation, flame topology and generated overpressure. For a given scale and with a single fixed and "well chosen" model constant, LES results match experimental findings, for all geometric arrangements of the obstacles and for methane, propane and hydrogen. However, when switching from small-scale cases to medium-scale or large-scale cases, this conclusion does not hold and the same model has difficulty capturing all scales without any coefficient change. This result illustrates one of the main deficiencies of these algebraic models, i.e. the need for an *a priori* fitting of the model parameters. At the same time, it also highlights the need for large variations of Reynolds and Damköhler numbers offered by the present database in order to correctly test models.

Possible solutions to overcome the limitations of algebraic models is to use mode refined models, such as the promising dynamic model recently developed by Wang *et al.* for instance [72, 20]. This model, taking advantage of the known resolved flow field to automatically adjust model parameters during the simulation, has the capacity of providing a much better precision over a wide range of scales. It is also *a priori* able to better handle out-of-equilibrium situations between turbulence motions and flame dynamics such as laminar-turbulent or turbulent-laminar transitions.

Acknowledgments

The authors thank Professor A. Masri (University of Sydney, Australia) and GexCon (Bergen, Norway) for providing experimental data. This work was supported by Total and ANRT under the CIFRE-2010-597. It was performed using HPC resources from GENCI-IDRIS (Grant 2013- x20132b5031). An award of computer time was provided by the Innovative and Novel Computational Impact on Theory and Experiment (INCITE) program. This research used resources of the Argonne Leadership Computing Facility, which is a DOE Office of Science User Facility supported under Contract DE-AC02-06CH11357.

References

[1] D. Bjerketvedt, J. R. Bakke, K. Van Wingerden, Gas explosion handbook, J. Hazard. Mater. 52 (1) (1997) 1–150.

[2] British Gas Review of the applicability of predictive methods to gas explosions in offshore modules, British Gas report for Department of Energy, OTH 89 312, London (1990).

[3] G. Ferrara, A. Di Benedetto, E. Salzano, G. Russo, CFD analysis of gas explosions vented through relief pipes, J. Hazard. Mater. 137 (2) (2006) 654–665.

[4] A. Di Benedetto, E. Salzano, CFD simulation of pressure piling, J. Loss Prevent. Proc. 23 (2010) 498–506.

[5] S. James, J. Zhu, M. Anand, Large eddy simulation as a design tool for gas turbine combustion systems, AIAA J. 44 (2006) 674–686.

[6] P. Moin, S. V. Apte, Large-eddy simulation of realistic gas turbine combustors, AIAA J. 44 (4) (2006) 698–708.

[7] L. Y. M. Gicquel, G. Staffelbach, T. Poinsot, Large eddy simulations of gaseous flames in gas turbine combustion chambers, Prog. Energ. Combust. Sci. 38 (6) (2012) 782 – 817.

[8] T. Poinsot, Prediction and control of combustion instabilities in real engines, Proc. Combust. Inst. doi:http://dx.doi.org/10.1016/j.proci.2016.05.007.

[9] O. Vermorel, S. Richard, O. Colin, C. Angelberger, A. Benkenida, D. Veynante, Towards the understanding of cyclic variability in a spark ignited engine using multi-cycle LES, Combust. Flame 156 (8) (2009) 1525–1541.

[10] C. Rutland, Large-eddy simulations for internal combustion engine - a review, Int. J. Engine Res. 12 (5) (2011) 421–451.

[11] D. Goryntsev, A. Sadiki, J. Janicka, Analysis of misfire processes in realistic direct injection spark ignition engine using multi-cycle large eddy simulation, Proc. Combust. Inst. 34 (2013) 2969–2976.

[12] G. Ciccarelli, S. B. Dorofeev, Flame acceleration and transition to detonation in ducts, Prog. Energ. Combust. Sci. 34 (4) (2008) 499–550.

[13] V. Di Sarli, A. Di Benedetto, G. Russo, Using Large Eddy Simulation for understanding vented gas explosions in the presence of obstacles, J. Hazard. Mater. 169 (1-3) (2009) 435–442.

[14] E. Oran, Understanding explosions – from catastrophic accidents to creation of the universe, Proc. Combust. Inst. 35 (1) (2015) 1–35.

[15] H. Pitsch, Large eddy simulation of turbulent combustion, Annu. Rev. Fluid Mech. 38 (2006) 453–482.

[16] H. Pitsch, L. D. de la Geneste, Large eddy simulation of premixed turbulent combustion using a level-set approach, Proc. Combust. Inst. 29 (2) (2002) 2001–2008.

[17] S. Richard, O. Colin, O. Vermorel, A. Benkenida, C. Angelberger, D. Veynante, Towards large eddy simulation of combustion in spark ignition engines, Proc. Combust. Inst. 31 (2007) 3059–3066.

[18] V. Moureau, B. Fiorina, H. Pitsch, A level set formulation for premixed combustion LES considering the turbulent flame structure, Combust. Flame 156 (4) (2009) 801–812.

[19] G. Kuenne, A. Ketelheun, J. Janicka, LES modeling of premixed combustion using a thickened flame approach coupled with FGM tabulated chemistry, Combust. Flame 158 (9) (2011) 1750 – 1767.

[20] G. Wang, M. Boileau, D. Veynante, Implementation of a dynamic thickened flame model for large eddy simulations of turbulent premixed combustion, Combust. Flame 158 (11) (2011) 2199 – 2213.

[21] A. N. Kolmogorov, The local structure of turbulence in incompressible viscous fluid for very large Reynolds numbers, Dokl. Akad. Nauk. SSSR 30 (1941) 301–305.

[22] T. Poinsot, D. Veynante, Theoretical and Numerical Combustion, Third Edition (www.cerfacs.fr/elearning), 2011.

[23] N. Peters, The turbulent burning velocity for large-scale and small-scale turbulence, J. Fluid Mech. 384 (1999) 107 – 132.

[24] F. A. Williams, Combustion Theory, Benjamin Cummings, Menlo Park, CA, 1985.

[25] N. Peters, Turbulent combustion, Cambridge University Press, 2001.

[26] J. Chen, Petascale direct numerical simulation of turbulent combustion—fundamental insights towards predictive models, Proc. Combust. Inst. 33 (2011) 99–123.

[27] J. E. Kent, A. R. Masri, S. H. Starner, S. S. Ibrahim, A new chamber to study premixed flame propagation past repeated obstacles, in: 5th Asia-Pacific Conference on Combustion, The University of Adelaide, Adelaide, Australia, 2005.

[28] A. R. Masri, A. Al-Harbi, S. Meares, S. S. Ibrahim, A comparative study of turbulent premixed flames propagating past repeated obstacles, Ind. Eng. Chem. Res. 51 (2012) 7690–7703.

[29] R. Starke, P. Roth, An experimental investigation of flame behavior during cylindrical vessel explosions, Combust. Flame 66 (1986) 249–259.

[30] M. Fairweather, S. S. Ibrahim, H. Jaggers, D. G. Walker, Turbulent premixed flame propagation in a cylindrical vessel, Proc. Combust. Inst. 26 (1996) 365–371.

[31] M. Fairweather, G. K. Hargrave, S. S. Ibrahim, D. G. Walker, Studies of premixed flame propagation in explosion tubes, Combust. Flame 116 (4) (1999) 504–518.

[32] H. Phylektou, G. E. Andrews, The acceleration of flame propagation in a tube by an obstacle, Combust. Flame 85 (1991) 363–379.

[33] R. Starke, P. Roth, An experimental investigation of flame behavior during explosions in cylindrical enclosures with obstacles, Combust. Flame 75 (1989) 111–121.

[34] R. P. Lindstedt, V. Sakthitharan, Time resolved velocity and turbulence measurements in turbulent gaseous explosions, Combust. Flame 114 (1998) 469–483.

[35] S. N. D. H. Patel, S. Jarvis, S. S. Ibrahim, G. K. Hargrave, An experimental and numerical investigation of premixed flame deflagration in a semiconfined explosion chamber, Proc. Combust. Inst. 29 (2002) 1849–1854.

[36] C. Johansen, G. Ciccarelli, Visualization of the unburned gas flow field ahead of an accelerating flame in an obstructed square channel, Combust. Flame 156 (2009) 405–416.

[37] T. Pinos, G. Ciccarelli, Combustion wave propagation through a bank of cross-flow cylinders, Combust. Flame 162 (2015) 3254–3262.

[38] R. G. Abdel-Gayed, D. Bradley, M. N. Hamid, M. Lawes, Lewis number effects on turbulent burning velocity, Proc. Combust. Inst. 20 (1984) 505–512.

[39] O. Gulder, Turbulent premixed flame propagation models for different combustion regimes, in: 23rd Symp. (Int.) on Comb., Vol. 23, The Combustion Institute, Pittsburgh, Orleans, 1991, pp. 743–750.

[40] A. Bonhomme, F. Duchaine, G. Wang, L. Selle, T. Poinsot, A parallel multidomain strategy to compute turbulent flows in fan-stirred closed vessels, Comput. Fluids 101 (2014) 183–193.

[41] S. R. Gubba, S. S. Ibrahim, W. Malalasekera, A. R. Masri, LES modeling of premixed deflagrating flames in a small-scale vented explosion chamber with a series of solid obstructions, Combust. Sci. Technol. 180 (10) (2008) 1936–1955.

[42] S. R. Gubba, S. S. Ibrahim, W. Malalasekera, A. R. Masri, An assessment of large eddy simulations of premixed flames propagating past repeated obstacles, Combust. Theor. Model. 13 (3) (2009) 513–540.

[43] S. R. Gubba, S. S. Ibrahim, W. Malalasekera, A. R. Masri, Measurements and LES calculations of turbulent premixed flame propagation past repeated obstacles, Combust. Flame 158 (12) (2011) 2465–2481.

[44] S. S. Ibrahim, S. R. Gubba, A. R. Masri, W. Malalasekera, Calculations of explosion deflagrating flames using a dynamic flame surface density model, J. Loss Prevent. Proc. 22 (3) (2009) 258–264.

[45] M. Abdel-Raheem, S. Ibrahim, W. Malalasekera, A. Masri, Large eddy simulation of hydrogen-air premixed flames in a small scale combustion chamber, Int. J. Hydrogen Energ. 40 (2015) 3098–3109.

[46] S. Roux, G. Lartigue, T. Poinsot, U. Meier, C. Bérat, Studies of mean and unsteady flow in a swirled combustor using experiments, acoustic analysis and large eddy simulations, Combust. Flame 141 (2005) 40–54.

[47] O. Colin, F. Ducros, D. Veynante, T. Poinsot, A thickened flame model for large eddy simulations of turbulent premixed combustion, Phys. Fluids 12 (7) (2000) 1843–1863.

[48] F. Charlette, D. Veynante, C. Meneveau, A power-law wrinkling model for LES of premixed turbulent combustion: Part I - non-dynamic formulation and initial tests, Combust. Flame 131 (2002) 159–180.

[49] V. Di Sarli, A. Di Benedetto, G. Russo, Sub-grid scale combustion models for large eddy simulation of unsteady premixed flame propagation around obstacles, J. Hazard. Mater. 180 (1) (2010) 71–78.

[50] X. Wen, M. Yu, Z. Liu, W. Sun, Large eddy simulation of methane-air deflagration in an obstructed chamber using different combustion models, J. Loss Prevent. Proc. 25 (2012) 730–738.

[51] P. Quillatre, Simulation aux grandes échelles d'explosions en domaine semi-confiné, Ph.D. thesis, Institut National Polytechnique de Toulouse (2014).

[52] P. Schmitt, T. Poinsot, B. Schuermans, K. P. Geigle, Large-eddy simulation and experimental study of heat transfer, nitric oxide emissions and combustion instability in a swirled turbulent high-pressure burner, J. Fluid Mech. 570 (2007) 17–46.

[53] N. Gourdain, L. Gicquel, M. Montagnac, O. Vermorel, M. Gazaix, G. Staffelbach, M. Garcia, J. Boussuge, T. Poinsot, High performance parallel computing of flows in complex geometries: I. methods, Comput. Sci. Disc. 2 (1) (2009) 015003.

[54] N. Gourdain, L. Gicquel, G. Staffelbach, O. Vermorel, F. Duchaine, J.-F. Boussuge, T. Poinsot, High performance parallel computing of flows in complex geometries - part 2: applications, Comput. Sci. Disc. 2 (1) (2009) 015004.

[55] O. Colin, M. Rudgyard, Development of high-order Taylor-Galerkin schemes for unsteady calculations, J. Comput. Phys. 162 (2) (2000) 338–371.

[56] N. Lamarque, Schémas numériques et conditions limites pour la simulation aux grandes échelles de la combustion diphasique dans les foyers d'hélicoptère, Phd thesis, INP Toulouse (2007).

[57] F. Ducros, F. Nicoud, T. Poinsot, Wall-adapating local eddy-viscosity models for simulations in complex geometries, in: ICFD, Baines M. J., 1998, pp. 293–300.

[58] B. Franzelli, E. Riber, M. Sanjosé, T. Poinsot, A two-step chemical scheme for Large-Eddy Simulation of kerosene-air flames, Combust. Flame 157 (7) (2010) 1364–1373.

[59] J.-P. Légier, T. Poinsot, D. Veynante, Dynamically thickened flame LES model for premixed and non-premixed turbulent combustion, in: Proc. of the Summer Program, Center for Turbulence Research, NASA Ames/Stanford Univ., 2000, pp. 157–168.

[60] D. Veynante, T. Poinsot, Effects of pressure gradients on turbulent premixed flames, J. Fluid Mech. 353 (1997) 83–114.

[61] C. R. Bauwens, J. Chaffee, S. B. Dorofeev, Vented explosion overpressures from combustion of hydrogen and hydrocarbon mixtures, Int. J. Hydrogen Energ. 36 (3) (2011) 2329–2336.

[62] C. Johansen, G. Ciccarelli, Modeling the initial flame acceleration in an obstructed channel using large eddy simulation, J. Loss Prevent. Proc. 26 (2013) 571–585.

[63] P. Wolf, G. Staffelbach, L. Gicquel, J.-D. Muller, T. Poinsot, Acoustic and large eddy simulation studies of azimuthal modes in annular combustion chambers, Combust. Flame 159 (11) (2012) 3398–3413.

[64] B. Enaux, V. Granet, O. Vermorel, C. Lacour, C. Pera, C. Angelberger, T. Poinsot, LES and experimental study of cycle-to-cycle variations in a spark ignition engine, Proc. Combust. Inst. 33 (2011) 3115–3122.

[65] A. Misdariis, O. Vermorel, T. Poinsot, A methodology based on reduced schemes to compute autoignition and propagation in internal combustion engines, Proc. Combust. Inst. 35 (3) (2015) 3001–3008.

[66] A. Roux, L. Y. M. Gicquel, Y. Sommerer, T. J. Poinsot, Large eddy simulation of mean and oscillating flow in a side-dump ramjet combustor, Combust. Flame 152 (1-2) (2007) 154–176.

[67] T. Poinsot, S. Lele, Boundary conditions for direct simulations of compressible viscous flows, J. Comput. Phys. 101 (1) (1992) 104–129.

[68] V. Granet, O. Vermorel, T. Leonard, L. Gicquel, T. Poinsot, Comparison of nonreflecting outlet boundary conditions for compressible solvers on unstructured grids, AIAA J. 48 (10) (2010) 2348–2364.

[69] P. Quillatre, O. Vermorel, T. Poinsot, P. Ricoux, Large eddy simulation of vented deflagration, Ind. Eng. Chem. Res. 52 (33) (2013) 11414–11423.

[70] V. Di Sarli, A. Di Benedetto, G. Russo, Large Eddy Simulation of transient premixed flame-vortex interactions in gas explosions, Chem. Eng. Sci. 71 (2012) 539–551.

[71] V. Di Sarli, A. Di Benedetto, Sensitivity to the presence of the combustion submodel for large eddy simulation of transient premixed flame–vortex interactions, Ind. Eng. Chem. Res. 51 (22) (2012) 7704–7712.

[72] G. Wang, M. Boileau, D. Veynante, K. Truffin, Large eddy simulation of a growing turbulent premixed flame kernel using a dynamic flame surface density model, Combust. Flame 159 (8) (2012) 2742–2754.

[73] P. Sagaut, Large Eddy Simulation for incompressible flows, Scientific computation series, Springer-Verlag, 2000.

[74] S. B. Pope, Ten questions concerning the large-eddy simulation of turbulent flows, New J. Phys. 6 (2004) 35.